Printing to Performance: A Review on 3D Concrete Printing Processes, Materials, and Life Cycle Assessment

Sanjeet Kumar Mishra[1], Snehal K[2], B. B. Das[*3], C Rajasekaran[4], Salim Barbhuiya[5]

[1]Research Scholar, Sustainable Construction and Building Materials Laboratory, Department of Civil Engineering, National Institute of Technology Karnataka, Surathkal, Karnataka, India, 575 025, E-Mail: sanjeetmishra93@gmail.com

[2]Assistant Professor, Department of Civil Engineering, Motilal Nehru National Institute of Technology Allahabad, Prayagraj, Uttar Pradesh, India, 211004, E-Mail: snehalshine090@gmail.com

[3*]Professor, Department of Civil Engineering, National Institute of Technology Karnataka, Surathkal, Karnataka, India, 575 025, E-Mail: bibhutibhusan@gmail.com

[4]Associate Professor, Department of Civil Engineering, National Institute of Technology Karnataka, Surathkal, Karnataka, India, 575 025, E-Mail: bcrajasekaran@gmail.com

[5]Senior Lecturer, Department of Engineering and Construction, University of East London, United Kingdom, University Way, London, E16 2RD, E-Mail: S.Barbhuiya@uel.ac.uk

*Corresponding Author

Abstract

A paradigm change in the construction sector has been sparked by the introduction of 3D concrete printing (3DCP), which provides cutting-edge alternatives to conventional building techniques. 3DCP is revolutionizing the construction industry by enabling automation, reducing material waste, and enhancing design flexibility. This review comprehensively explores the working principles, types of printers, and various printing methods used in 3DCP. The operational aspects, including advancements in printhead systems and the impact of key parameters such as nozzle shape, size, printing height, speed, and interlayer gap time, are examined to understand their influence on both fresh and hardened properties of printed concrete. The mix design strategies for sustainable material selection are critically reviewed, focusing on optimizing rheology, printability, and mechanical performance. Furthermore, the study discusses the durability aspects and microstructural characteristics of 3D-printed concrete, highlighting reinforcement techniques and embedment methods. This review also looks at the life cycle analysis of 3D-printed concrete buildings, emphasizing the enormous cost and CO_2 reduction potential of eliminating formwork, which results in an 89.2% reduction in CO_2 production and a 30-40% reduction in structure cost. The environmental impact of 3DCP techniques compared to traditional construction is explored, taking into account factors such as energy usage, trash production, and carbon footprints. In conclusion, this review serves as a valuable resource for researchers and industry professionals, offering a comprehensive understanding of the latest advancements, challenges, and future directions in 3D concrete printing.

Keywords 3D concrete printing, printing parameters, material selection, mix design, rheology, life cycle analysis

Highlights

- A comprehensive review of working principles, types of printers, methods of printing, operation, sustainable material selection, mix design, and life cycle analysis is presented.
- Steps involved in 3D concrete printing are discussed in detail.
- Types of printers and their use are reviewed.
- Advancements in printhead systems were explored.
- The influence of nozzle shape, size, printing height, printing speed, and interlayer gap time on the fresh and hardened characteristics are studied.
- Early-age and harden properties of 3D printable concrete are discussed.
- Durability and micro-structural analysis are presented.
- Different types of reinforcement and their embedment methods are discussed.
- Life cycle assessment and life cycle costing are presented.

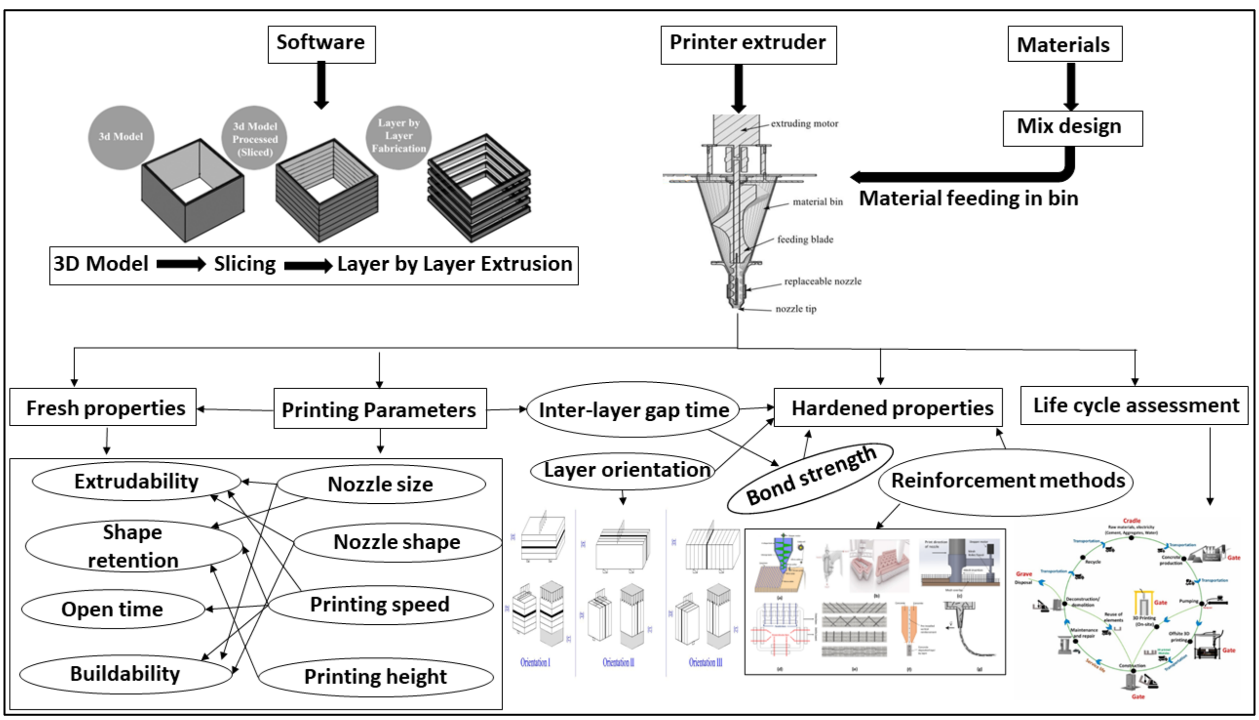

Graphical abstract

1 Introduction

The construction sector has recently undergone a dramatic upheaval with the advent of 3DCP technology [1]. A cutting-edge building technique called 3DCP, sometimes referred to as additive manufacturing in the industry, builds three-dimensional structures layer by layer using robotics and computer-aided design [2]. Due to its unparalleled levels of design flexibility, economic effectiveness, and sustainability, this novel methodology has the potential to challenge conventional construction methods. Three-dimensional printing (3DP) is a promising technology that fabricates concrete structures without using formwork [2]. This novel technology has the potential to alter design, speed, labor cost, accuracy, efficiency, sustainability, integration of functions, low production waste, and maintenance practices in construction industry. This technology is said to reduce production time by 50–70%, labor costs by 50–80%, construction waste by 30–60%, and environmental impact by 50% [3, 4]. The ability to complete unique geometric complexity and lean bespoke building is one of this technology's main advantages. Other key advantages include digitization, individualization, and automation in the construction business. Three primary techniques are now used in 3DCP: a) material extrusion, b) material spraying, and c) particle bed binding [5]. Extrusion 3DCP is the most popular technique used in construction, where layers of a plastically malleable cementitious composite material are applied [2]. Fig. 1 compares the construction process between the conventional construction method and 3DCP.

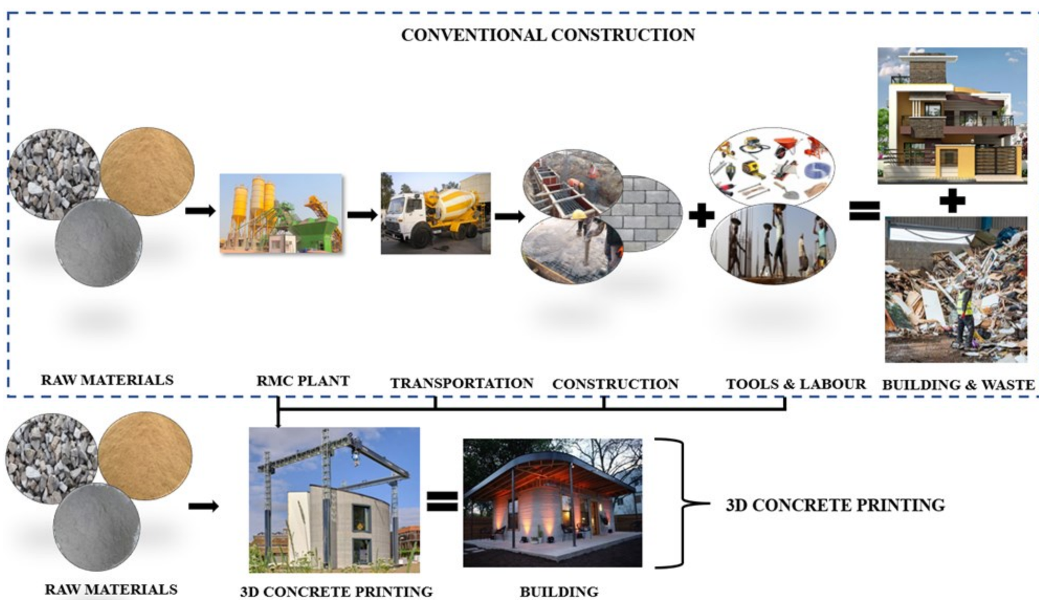

Fig. 1 Comparison of the construction process between conventional construction method and 3D concrete printing

Around the world, remarkable constructions like homes, offices, pavilions, bridges, and more have been built using 3DCP technology. The UAE government has mandated the use of 3DCP for government facilities, and India has shown interest in using it for railways, post offices, and defense sectors.

The emerging domain of 3D concrete printing offers several prospects for research and advancement; however, there are several research gaps that require attention. Sustainability is paramount, with a pressing need to reduce environmental effects. This can be accomplished by including alternative and recycled materials, reducing energy consumption during printing, and adopting ways for recycling or reusing printed materials [6, 7]. Moreover, the current lack of reinforcement in many 3D-printed concrete structures imposes limitations on their structural capacities, necessitating inventive approaches for the incorporation of reinforcement during the printing procedure [8, 9]. Additionally, the pace of printing and the ability to scale up structures remain formidable challenges [10, 11]. Present methods often suffer from slow printing speeds and constraints on the size of printable structures, necessitating advancements in these areas to realize the technology's full potential. Significantly, as the adoption of 3D concrete printing grows, there is an increasingly urgent requirement for standardization and regulation. Implementing standardized methods, protocols, and rules is crucial to ensuring quality control, safety, and synchronization with existing construction methodologies. The potential of 3D concrete printing can only be realized via focused and collaborative efforts to solve these research gaps.

In this era of quick technical development, an in-depth knowledge of the complexities and effects of 3DCP is crucial. This review intends to look deeply into the many aspects of 3DCP, encompassing its mechanism, operation, material choice, and life cycle analysis (LCA). By breaking down each of these crucial components, this paper aims to offer a thorough and perceptive understanding of this revolutionary construction method.

2 Working mechanisms of 3D concrete printing

The 3D concrete printer functions similarly to Fused Deposition Modeling (FDM) printers, using G-code to control the print head's movement along three axes (X, Y, Z). The process involves four stages: 3D modeling, slicing, printing, and post-processing. 3D CAD software is commonly used to create models, which are then converted into STL files [12]. Slicing software breaks the model into 2D layers, and printing parameters like the printhead speed, extrusion rate, layer height and rate of binder deposition are sent to the 3D printer in the form of a G-code. The printer constructs the structure layer by layer according to these defined parameters [13].

Fig. 2 presents the flow of the working mechanism of a typical 3D concrete printer.

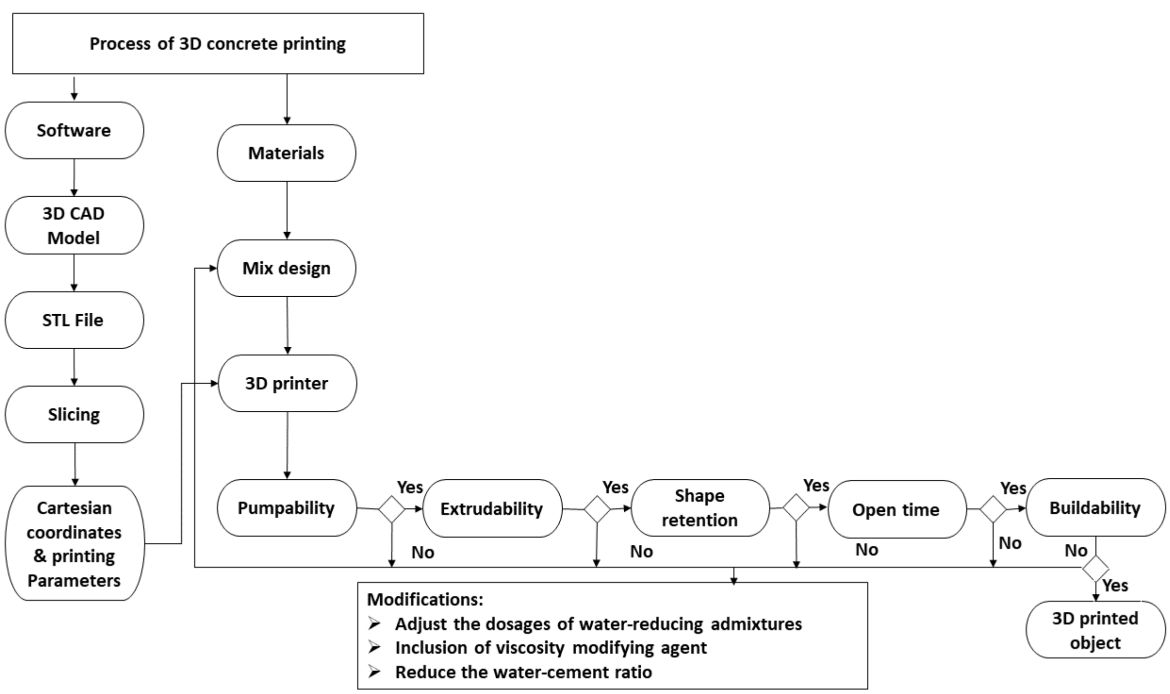

Fig. 2 Steps involved in 3D concrete printing

3 Fabrication using a 3D concrete printer

3D concrete can be printed using two methods: in-situ and prefabrication. Prefabrication involves printing parts in a factory before shipping them for assembly on-site. In-situ printing installs the printer on-site to print the entire structure as a single unit [14].

The leading 3D printing techniques are contour crafting, concrete printing, and D-shape. Contour crafting uses material extrusion and computer programs to create smooth surfaces [15]. It begins by printing the outer edges of a structure and then filling it with concrete. This method is suitable for large-scale projects but is limited in developing tall structures due to its horizontal extrusion approach. It is more limited in developing tall, vertical structures than other methods [15, 16].

The D-shape method employs powder and binder. First, a layer of powder is spread through the nozzle mounted on the printing head. Then, the chemical agent is spread over the powder through another nozzle, requiring 24 hours for solidification after application, making it ideal for medium-sized structures [16]. Concrete printing, similar to contour crafting, allows for more complex shapes and can be used for both on-site and prefabricated construction. Various 3D concrete printers, including gantry, robotic arm, mobile, compound arm, and delta-style printers, are classified based on size and site conditions [11].

In-situ printing is effective for larger projects but can be affected by weather, while prefabrication offers creative shapes but comes with higher geometric complexity [14]. Some projects combine both methods and leading construction companies (PERI, Apis cor, ICON, COBOD) recommend specific printers and fabrication systems for different construction types [17, 18], which is presented in Table 1.

Table 1 Recommendation of printers and fabrication systems for different types of construction [19]

Construction type	Fabrication type	Printer type	Advantages	Company
An array of low-rise building	On-site printing	Mobile gantry	Capability to print many buildings in-one-go	ICON Technology (n.d)
Single low-rise buildings with huge footprint	On-site printing	Mobile robotic arm	Flexibility while moving inside the building	TsingHua University
Low-rise buildings with dome shape roofs	On-site printing	Mobile robotic arm	Enabling the printing of walls and roofs separately	Tsinghua University
The bearing walls of low-rise houses	On-site printing	Gantry type	High efficiency and the capacity to print multiple structures at once	ICON, COBOD, PERI Group
Arch/vault bridges	Prefabrication	Robotic arm	Allowing printing with different layer heights	Block Research Group, Zaha Hadid Architects and Incremental 3D

Flat bridge	Prefabrication	Gantry type	Manipulation is simple	Eindhoven University of Technology
Complex/irregular structures	Prefabrication	Robotic arm	Allowing printing with different layer heights	RMIT, Fab Union, Tsinghua University

In conclusion, 3D printing provides a diverse range of approaches and strategies, ranging from contour crafting to concrete printing and D-shape technology. Balancing factors such as workspace efficiency, geometric complexity, and environmental concerns helps determine whether in-situ or prefabrication processes are preferable. In-situ printing allows for on-site customization, reduces transportation costs, and enables rapid construction. Meanwhile, prefabrication ensures quality control, precision, and flexibility in scheduling. The choice between the two depends on the project scale, timeline, budget, and specific needs. Overall, 3D printing can revolutionize construction by integrating the strengths of both approaches.

4 Printing parameters

The size and shape of the nozzle, printing height, extrusion velocity and printing speed are critical printing characteristics that have a significant impact on printing quality. Different geometry of the nozzles, printing height, and its effect on printing are shown in Fig. 3 and Fig. 4, respectively.

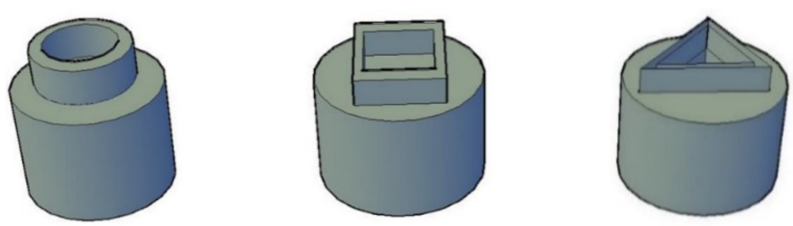

(a) (b) (c)

Fig. 3 Different shapes of the nozzles a) circular, b) rectangular, and c) triangular

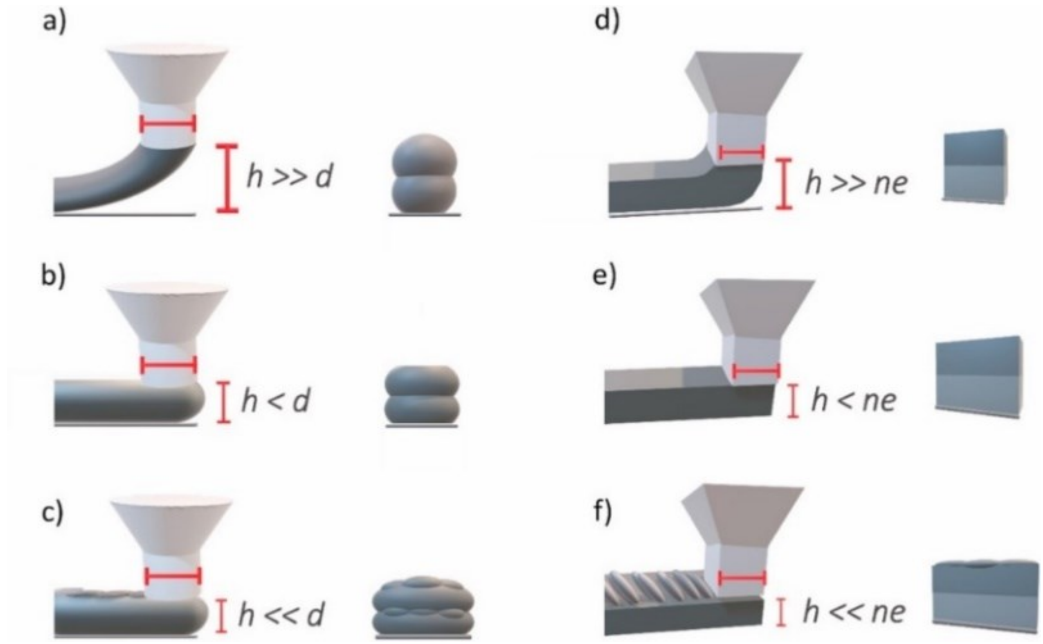

Fig. 4 Effect of nozzle geometry and layer height on the printed layer [17]

The study by Zhang and Sanjayan (2023) investigates the relationship between nozzle dimensions, printing parameters, and filament dimensions to enhance the quality of 3D concrete printing. They identified four key factors influencing extrusion resistance: wall friction, die friction, shaping pressure, and conical friction stress [20]. Minimizing nozzle length and extrusion velocity is essential for reducing resistance. Moreover, screw-type nozzles are highlighted for their ability to uniformly extrude cementitious materials by applying shear and axial pressure, improving compactness and extrusion efficiency [21]. A typical Auger screw with a total length (L) of 300 mm; pitch (Pc) of 48 mm; diameter (D) of 50 mm; and blade angle of 19° is shown in Fig. 5 [22].

The study also emphasizes the impact of layer height on surface quality and bonding. A higher printing height decreases interfacial bonding strength, leading to instability, while a lower height can cause deformation from high nozzle pressure [23].Wolfs et al. [24] suggested that nozzle width and printing height should match to ensure smooth mortar layers and prevent contact between the print head and the surface. Other researchers noted that interlayer bond strength improves when the nozzle height is less than the strip height, and a layer height between 10 mm and 15 mm with a 30 mm circular nozzle is ideal for optimal adhesion [25]. Xiao et al. [21] found that a higher layer height (25 mm) results in curved surfaces that weaken bonding, while a smaller height can cause excess material accumulation.

Moreover, the shape of nozzles significantly affects interlayer bonding. Rectangular nozzles yield better mechanical properties than circular ones due to reduced gaps, though circular nozzles are better for complex structures [26]. Triangular nozzles exhibit minimal interlayer defects under similar conditions [27]. The relationship between nozzle height (h) and diameter (d) alters layer quality, where $h \geq d$ results in reduced contact area, and $h < d$ produces more stable layers [17]. Circular nozzles (Fig. 4a) cause rounded top and side printed layers if $h \geq d$, reducing layer-to-layer contact area and interlayer bond. A flattened top surface and rounded sides occur if $h < d$ (Fig. 4b) [17]. If $h \ll d$, the printed layer tends to be pushed back and to the sides, generating deeper layers with the possibility of ripple-type flaws (Fig. 4c). Whereas the rectangular nozzle enables flat layers on sides and top even if h is greater than nozzle edges (ne) (Fig. 4d). Thicker layers can be produced by maintaining speed and adjusting "h" to be slightly less than 'ne' (Fig. 4e). However, the possibility of flaws increases when h << ne (Fig. 4f).

Print head speed, essential for material deposition, influences fresh properties, interlayer bond strength, and the geometry of printed layers. Adjusting extrusion speed according to print head speed helps maintain layer stability [28]. Xiao et al. advised matching extruding speed with travel speed to ensure consistent layer thickness and width, as an increased speed can decrease layer stability. However, slow speeds may lead to material accumulation [21]. Also, the interlayer tensile bonding strength of the specimen reduces as the print speed increases [25].

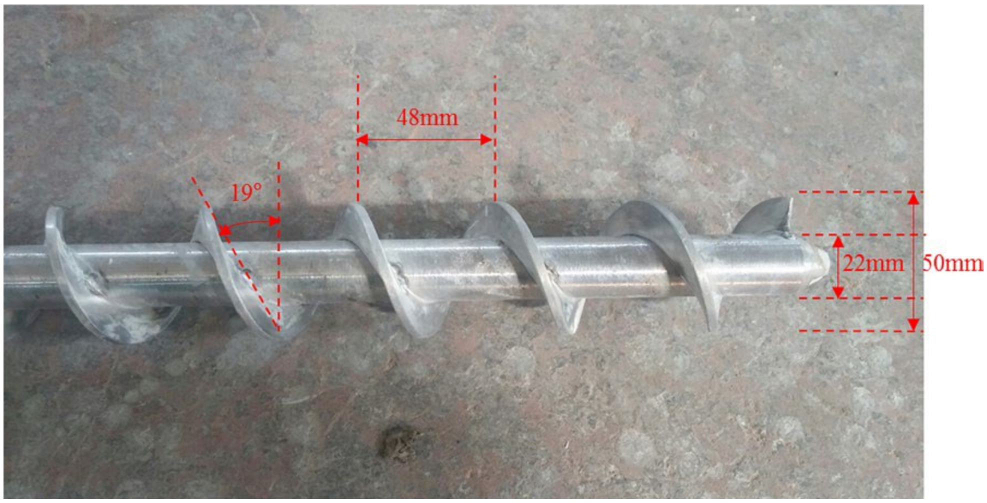

Fig. 5 Designed screw (Auger) for nozzle [22]

A suggested formula, as mentioned in Equation 1, shows the relationship among extrusion velocity, nozzle dimensions, and printing parameters that provides a prediction tool for maintaining consistent print quality. These findings collectively underline the need to adjust nozzle design, printing height, nozzle shape, flow rate, and speed to produce optimum 3D printing quality [20].

$$W_m = \frac{\frac{\pi (N_D)^2 V}{4 H_{nl} S_p} + k N_D}{1 + k} \quad ---------(1)$$

Where, Wm is the filament width, N_D is the nozzle outlet diameter, V is the extrusion velocity, H_{nl} is the nozzle lift height, S_p is the printing speed, and k is a parameter reflecting deviations between experimental and calculated data.

The nozzle and extrusion system described is suitable for concrete printing and contour crafting, as they use similar extrusion principles. However, these methods do not apply to D-shape printing, which uses a different mechanism involving particle jetting and requires a printhead for liquid binder deposition. Consequently, this review will focus exclusively on extrusion-based 3D concrete printing properties. Researchers' suggestions on parameters like nozzle shape, size, printing height, flow rate, and speed are summarized in Table 2.

Table 2 Printing parameters and their effect on the 3D-printed concrete

References	Types of nozzles	Size of nozzles	Flow rate	Printing height	Printing speed	Remarks
Tay et al. [29]	Rectangular	30x15 mm^2	37.9 ml/s, 45.2 ml/s, 48 ml/s, 51.3 ml/s	15 mm	60-200 mm/s	- No breaks and cracks were seen at a flow rate of 48 ml/s and 51.3 ml/s till the printing speed of 100 mm/s. - At flow rates of 37.9 ml/s, 45.2 ml/s breaks or cracks started at 60 mm/s.
Manikandan [30]	Square and Circular	6x6 mm^2, and 6 mm diameter	20 mm/s (Extrusion speed)	-	15 mm/s	- The compressive strength of a cylindrical specimen printed using a square nozzle is more than that of a specimen printed using a circular nozzle.
Lu et al. [31]	Spray nozzle	-	1.8 lit/m and 3.6 lit/m	50 mm, 70 mm, and 100 mm	20-250 mm/s	- Width and thickness of filament increased with flow rate. - Width of the layer increased but the thickness was reduced by increasing the nozzle height. - Thickness and width initially decreased by increasing nozzle speed, but a further increase in the speed reduced this effect.
Panda et al. [23]	Square	20x20 mm^2	Optimum level	15 mm and 20 mm	Optimum level	- Height has a negligible effect on bond strength in the control mix. - At 15 mm printing height, the mix prepared using nano clay has 33% higher bond strength than the one with 20 mm printing height.
Panda et al. [25]	Rectangular and square	-	1.5 lit/m	0 mm, 2 mm, 4 mm	70 mm/s, 90 mm/s, 110 mm/s	- Smaller bead width was observed for higher printing speed. - Bond strength of the printed layers reduced at a printing speed of 110 mm/s. - With an increase in printing height, bond strength decreased.

Paul et al. [26]	Rectangular and circular	10x20 mm^2 and 8 mm diameter	3 lit/m	-	-	- Strength is higher in the case rectangular nozzle due to the less interlayers gap as compared to the circular nozzle. - In addition, more voids are formed in a circular nozzle which also results in less strength. - Circular nozzle is suitable for printing complex structures.

In addition to the extrusion systems discussed above, the following sections introduce advancements in printhead systems that are widely used in modern 3D concrete printing.

4.1 Advancements in printhead systems

Advancement in printhead technology have substantially boosted the scalability, efficiency, and material uniformity of 3D concrete printing (3DCP). These advances tackle issues including ensuring the retention of material fluidity during pumping and the attainment of fast stiffening after extrusion. Traditional single-component systems, though effective for small-scale applications, often struggle with large-scale operations. To overcome these limitations, several advanced technologies have been developed which are discussed below.

Dual head extrusion

Dual head extrusion in 3D concrete printing involves the simultaneous deposition of two different materials or the same materials at two different places through separate print heads, enabling the fabrication of structures with enhanced properties and functionalities. This innovative method combines several concrete mixes, reinforcing fibers, or even additional materials like waterproofing or insulation into a single printed object [32]. Ji et al. [33] designed a double-headed 3D concrete printer capable of printing ready-mix concrete. A schematic representation of the double print head is shown in Fig. 6 (a).

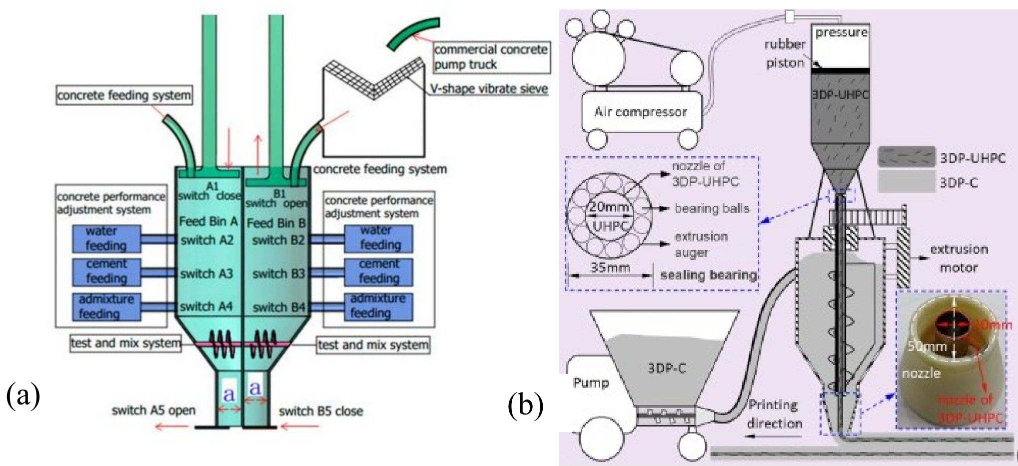

Fig. 6 Schematic of (a) Piston based [33] **and (b) Extrusion based dual head** [32]

The print head comprises two feed bins, each with four systems: a reciprocating plugging power system, a concrete performance adjustment system, a concrete feeding system, and a test and mix system. This design allows for the simultaneous operation of feed bins A and B, enabling continuous concrete printing. In feed bin A, piston A descends to extrude concrete while piston C opens switch A5 to facilitate this process. At the same time, piston D moves upward to activate switch B5, feeding concrete into feed bin B.

Another dual-head printing system developed by Bai et al. [32], illustrated in Fig. 6(b), prints ordinary concrete (3DP-C) and ultra-high-performance concrete (3DP-UHPC) concurrently. It features a spiral extrusion mechanism for standard concrete and a pressure-regulated piston for UHPC, which reinforces the mix. The UHPC-reinforced concrete achieved a 160.5% increase in ultimate bending strength compared to non-reinforced 3DP-C.

Twin-pipe pumping strategy

In this novel method, Tao et al. [34] utilised two independent pipes to convey two different mixtures—a cement-based mixture without an accelerator and a limestone-based mixture with a substantial accelerator dose. The mixes were combined in a static mixer adjacent to the nozzle, as shown in Fig. 7. The limestone-based mix had a long open time and high fluidity and was meant to stay inert throughout pumping. Upon combining with the cement-based mixture in the nozzle, stiffening is promptly started, ensuring excellent shape stability and speedy layer-by-layer building. This approach has shown the ability to print a 3-meter-high column and efficiently balance pumping efficiency with buildability.

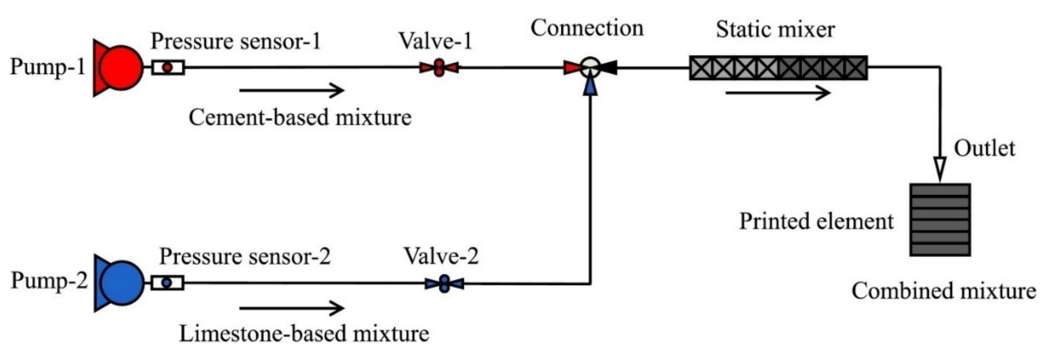

Fig. 7 Schematic illustration of twin-pipe pumping technique [34]

Inline 2K component systems

These systems use secondary mixing near the nozzle, as shown in Fig. 8, to introduce additives like accelerators or other chemical admixtures. Wangler et al. [35] underline the necessity of inline mixing for preserving homogeneity and minimising material deterioration during transit. By permitting accurate mixing and eliminating dead zones, these systems solve fundamental issues in large-scale 3DCP, such as maintaining material rheology and achieving effective hydration control. The inline 2K system has been particularly effective in scaling the process to more significant print areas and higher flow rates, making it ideal for structural-scale applications.

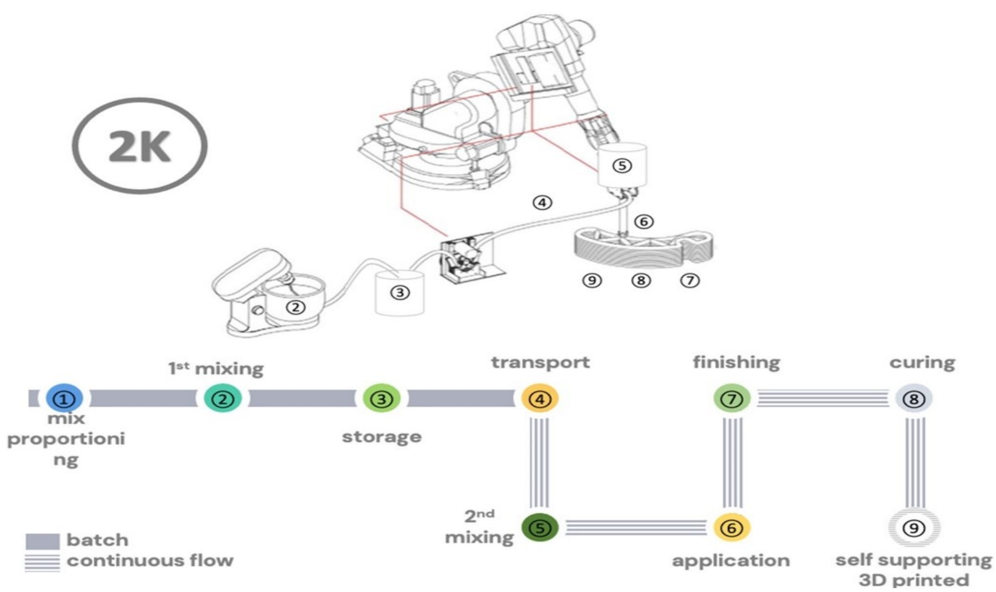

Fig. 8 2K mixing component systems [35]

Quick nozzle mixing

A pumping-less approach that combines dry and liquid components right away at the nozzle, this technology streamlines the process and eliminates material waste. It removes the necessity for carrying wet concrete, hence lowering cleaning efforts and process inefficiencies. Although this technique enhances automation and resource usage, difficulties like anisotropic strength in printed structures remain a barrier. Zhang and Sanjayan [36] underline its potential for improving flow rates and retaining control over rheological properties, opening the path for more simplified 3DCP processes. A schematic representation of the quick nozzle mixing process is shown in Fig. 9.

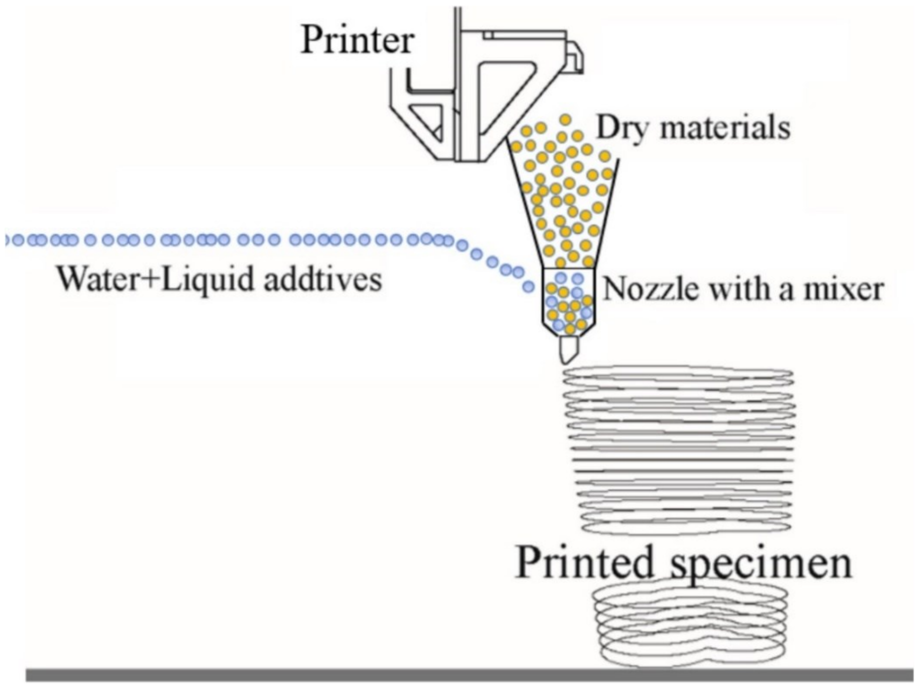

Fig. 9 Schematic of quick nozzle mixing process in 3DCP [36]

Short-duration mixing near the nozzle

This approach assures consistent rheological qualities and effective hydration control by lowering residence time and limiting dead zones in the mixing process. Zhang et al. [37] emphasise the value of near-nozzle dynamic mixing in attaining improved material placement and reducing processing pathologies. This method optimises the consistency of material extrusion, which is crucial for large-scale 3DCP applications. It tackles common challenges such as material segregation and uneven distribution, leading to enhanced structural performance.

5 Material selection and mix design approach

The 3DCP technology in construction requires concrete with specific rheological properties, significantly influenced by mix proportions [38]. Admixtures such as high-range water-reducers, viscosity-modifying admixtures, accelerators, retarders, superplasticizers, alkali activators, nanomaterials, and fibres are commonly incorporated to enhance these properties [39, 40]. Binder systems typically consist of OPC [41, 42] supplemented with fly ash [43, 44], silica fume [43, 45], calcined clay, and limestone [46, 47], which improve early-age strength and durability and mitigate phase separation. However, 3D printable mixes contain higher binder content, making alternative binders like alkali-activated materials and geopolymers more sustainable [40, 45, 46]. Coarse aggregates are avoided due to potential clogging during extrusion; fine aggregates with a particle size of less than 2 mm are preferred for better workability and surface finish [48]. The use of 100% recycled sand can reduce fluidity and flow retention in printing mortar, but incorporating sodium gluconate as a retarder improves these properties [49]. This combination enhances stiffness and compressive strength, facilitating efficient 3D printing. Particle packing theory is critical in optimizing 3DCP mixes.

Particle packing theory

Particle packing models aim to fill larger voids by selecting appropriate quantities and ratios of smaller particles, which fill the spaces between them [50]. Enhancing aggregate gradation increases packing density, reducing the cement paste needed to fill voids. This method promotes sustainable development and enhances concrete performance by creating a denser solid network and reducing interparticle spacing [51]. The packing density also influences the rheological and flow characteristics of concrete mixes [52]. Researchers have introduced active pozzolanic materials, like silica fume and nanoscale particles rich in amorphous SiO_2, to improve packing density and mechanical properties. As the silica fume concentration increases from 0 to 15%, the packing density is enhanced and fills the gaps with finer particles [53]. Fig. 10 shows the packing density of mixes with silica fume (SF), calcined clay (CC), and limestone (LS).

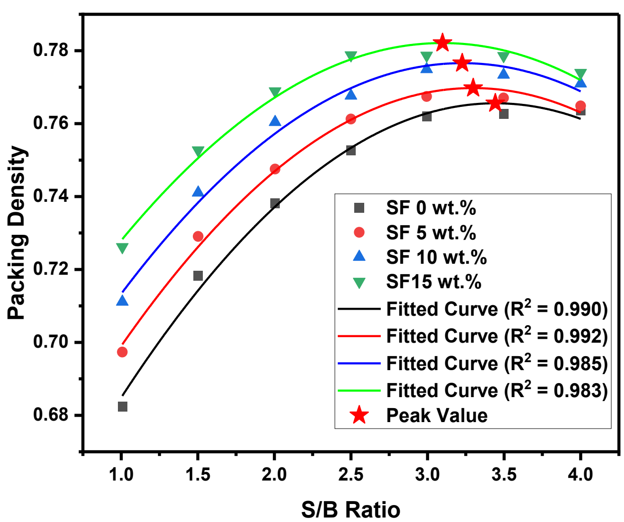

★ Peak Value

SF (%)	S/B ratio	Packing density
0	3.442	0.765
5	3.299	0.769
10	3.227	0.776
15	3.098	0.782

(a)

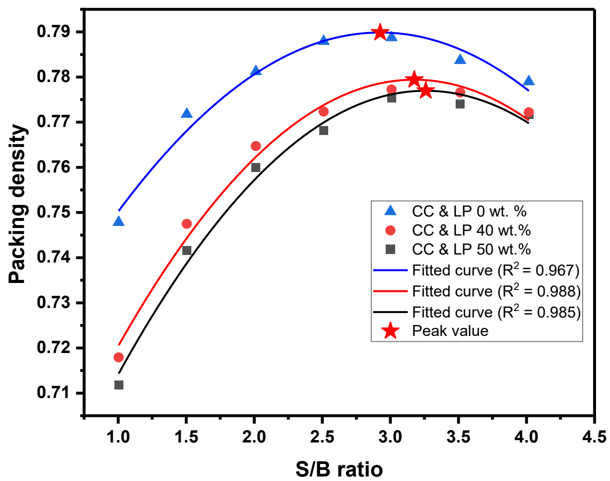

★ Peak value

CC & LP (%)	S/B ratio	Packing density
0	2.925	0.789
40	3.175	0.779
50	3.26	0.776

(b)

Fig. 10 Different mixes' packing density: (a) Effect of S/B ratio and SF% when CC and LP% were fixed at 50% on packing density; (b) Effect of S/B ratio and CC and LP% when SF% was fixed at 10% on packing density [54]

Although calcined clay has a smaller particle size than cement, the increase in calcined clay (CC) and limestone powder (LP) exhibited poor packing density (Fig. 11) [54, 55]. The lowest packing density were observed at sand-binder (S/B) ratios of 1. However, an increase in the S/B ratio and SF dosage resulted in higher packing density values, but the trend was reversed for CC and LP mixes [54, 55]. Attempts to use aggregates as large as 20 mm in 3D concrete printing (3DCP) resulted in a decline in print quality and an increase in void volume. Better print quality may be achieved with improved particle packing with a larger aggregate size [56]. The modified Andreasen and Anderson model (Equation 2) was used to find the target particle size distribution curve and determine the mix proportion of 3D printed ultra-high-performance fiber-reinforced concrete [57].

$$P_{tar}(D) = \frac{D^q - Dmin^q}{Dmax^q - Dmin^q} - - - - - - -(2)$$

Where D is the particle size, P_{tar} (D) is the volume proportion of all solids smaller than D, and D_{min} and D_{max} are the minima and maximum particle sizes of the mix, respectively. The distribution modulus (q) is a parameter that controls workability, and q = 0.23 was suggested for the production of UHPFRC mixes [57].

The optimum proportions of printable mixes and various binding materials, fine aggregates, water-binder ratios, and sand-binder ratios, fibers, and additives used by different researchers are discussed in Table 3.

Table 3 Materials and mix design approach for 3D concrete printing

Mix Type	Binder used	W/B ratio	S/B ratio	Sand size (mm)	Fiber (%) **	Admixture (%) **	Ref.
Cement-based mix	OPC	0.36	2			HRWRA = 0.15	[58]
	OPC	0.39	1.2	0-0.9		HRWRA = 0.13 VMA = 0.18	[41]
	OPC	0.36	1.5	0-2	-	-	[42]
	OPC	0.28	1	0-2		WRA = 0.471 Retarder = 0.5	[59]

	OPC	0.41	1	0-0.1	-	HRWRA = 0.3	[60]
	OPC	0.49	1	0-0.9 (RS)		SP = 0.08 VMA = 0.12 Retarder = 0.12	[49]
Cement-SCM blended mix	OPC, GGBS, SF, SS (0.695:0.20:0.10:0.05)	0.4	-	0-1.18	-	WRA = 0.3	[40]
	OPC, SF	0.34	1.8	-	-	WRA= 0.7 VMA = 0.004	[61]
	OPC, SF, FA, SAC	0.3	0.40	CA = 5-10	0.2	VMA = 0.05	[45]
	OPC, FA	0.31	0.9 Glass/ Binder	0-1.7 (RGS)	-	VMA = 0.2	[62]
	OPC, FA (0.75:0.25)	0.32	1.5	-	PP fiber = 1.8 kg/m^3	PCE based superplasticizer = 0.08 VMA = 0.25	[63]
	OPC, SF, BSAC (0.85:0.1:0.05)	0.37	1.3	0-0.55	-	WRA-PCE = 0.43	[64]
	OPC, FA, SF (0.26:0.26:0.48)	0.42	1.54	0-2	-	HRWRA = 2-3	[43]
Geopolymer mix	FA, GGBS (1:1)	0.4	1.5	-	-	Activator/Binder = 0.35	[65]
	FA, GGBS (0.50:0.50)	0.36	1.5	-	-	Retarder = 0.5, Alkali activator = 10	[39]
MPCCs	M/P mass ratio of 3.0, 25% FA, and 40% borax	0.12	FA/B = 0.25	-	-	RMA = 0.5,	[44]
Engineered cementitious composites (ECC)	OPC, SAC, SF, FA (0.38:0.05:0.09:0.48)	0.26	0.40	0-0.3	1.8	SP = 0.1	[66]
	OPC, CAC, FA, (0.30:0.02:0.68)	0.25	0.38	-	PVA fiber = 2	VMA = 0.3, Nano-clay = 0.3, nano-TiO2 =5, HRWRA = 0.9	[67]

**%Wt. of binder, S/B- Sand-binder ratio, W/B- Water-binder ratio, RS- 100% recycled sand, RGS- Recycled glass sand, CA- Coarse aggregate, GGBS- Ground granulated blast furnace slag, SF- Silica fume, OPC- Ordinary Portland cement, FA- Fly ash, MK- Metakaolin, SS- Sodium Metasilicate, PP- Polypropylene fiber, PVA- polyvinyl alcohol, SAC- Sulfoaluminate cement, BSAC- Belite sulfoaluminate cement, CAC- Calcium Aluminate cement, SP- Superplasticizer, PCE- Polycarboxylate ether, VMA- Viscosity modifying admixtures, HRWRA- High-range water-reducing admixtures, WRA- Water reducing admixture, RMA- Rheology modifying admixture, MPCCs- Magnesium potassium phosphate cement composites, M/P- Magnesium-potassium ratio.

In conclusion, achieving the desired stiffness and shape stability in 3D printable mixes relies on precise adjustments to water-binder and sand-binder ratios, with fibers and viscosity-modifying admixtures (VMAs) playing a crucial role in reducing layer deformation. The use of supplementary cementitious materials (SCMs) like fly ash, metakaolin and silica fume improves strength, durability, and rheological properties while enhancing sustainability. Additionally, particle packing theory optimizes mix design by increasing packing density through the careful gradation of particle sizes, reducing the need for excess cement paste. This approach, along with proper binder selection and aggregate gradation, enhances both print quality and overall performance in 3D concrete printing.

6 Early age properties of a 3D printable mixture

The properties of 3D printable mortar at an early age are essential for assessing the effectiveness of the printing process and the integrity of the printed structure. These properties, which include pumpability, extrudability, shape retention, open time, and buildability, directly influence the material's ability to be transported, shaped, and sustain its form during and after printing [68]. Investigating these properties at an initial phase is essential for multiple reasons. At first, they facilitate efficient material handling throughout the printing process, mitigating problems such as clogging or inconsistent extrusion that may result in defects. Secondly, the assessment focuses on the material's capacity to uphold structural integrity throughout the layer deposition process, preventing any collapse or deformation, thereby ensuring both dimensional accuracy and stability [13, 60]. Controlling these properties facilitates the optimisation of the printing process regarding speed, efficiency, and quality. This enables a balance between flow properties and early structural strength. Each subsequent subsection provides a detailed examination of these key properties, emphasising their significance in 3D concrete printing and the methodologies employed for their assessment and optimisation.

6.1 Pumpability

In 3DCP, pumpability refers to the ability to deliver fresh cementitious material from the pump to the nozzle [69]. Inappropriate mix design and pumping rates can lead to problems such as excessively high pumping pressure, pipe clogging, material spilling, and grain separation during pumping [70]. Several variables, including aggregate size, sand-binder ratio, water-binder ratio, admixture dosage, flow rate, height and distance to pump, hose diameter, etc., affect the pressure required for pumping are presented below in Table 4 [70]. For instance, Mohan et al. [71] evaluated the pumpability of the mixture with an aggregate size of 2 mm, using a rubber hose diameter of 30 mm and length of 5 m, until the flow rate was consistent and uniform. They found that as aggregate size increased, pumping pressure also increased. Several trial-based methods have been developed for measuring pumpability, including using a rotor and stator pump to provide suitable supply rates for 3DCP [72]. The sliding pipe rheometer (SLIPER) developed by Mechtcherine et al. [73, 74] calculates the flow rate by measuring the weight of the mixture delivered at a constant speed for a fixed duration using the mixture weight and density as volume per second [75]. Researchers have also used the Bingham model to analyze pumpability by measuring the pumping pressure (P) of cementitious materials, which is described in Equation 3 [76].

$$P = \left[\frac{8\tau_d}{3R} + \frac{8\mu}{\Pi R^4} Q\right] L ------(3)$$

In this equation, Q represents the flow rate of the materials, L represents the length of the hose, R is the radius of the hose, μ is the plastic viscosity, and τ_d represents the dynamic yield stress of the materials.

Table 4 Factors Influencing Pumpability in 3DCP

Factors Affecting Pumpability	Remarks	References
Aggregate Size	Fine aggregates reduce friction and allow smoother flow, while coarser aggregates can lead to clogging.	[70, 71]
Sand-Binder Ratio	An adequate sand-binder ratio ensures the required cohesion; however, an excess of sand might hinder flowability and raise pressure levels.	[71, 77]
Water-Binder Ratio	A higher water-binder ratio reduces viscosity, making the mix easier to pump. However, excess water can cause segregation.	[75, 77]
Admixture Dosage	Admixtures like superplasticizers improve workability and lower water requirements, but excessive dosage might result in segregation.	[78, 79]
Flow Rate	Controlled flow rates provide consistent pumping free of obstructions, while excessively high flow rates might result in pump blockage.	[74]
Height and Distance to Pump	Longer distances or higher elevations lead to increased pressure loss, making pumping more challenging.	[73, 74]
Hose Diameter	Wider hoses reduce resistance and ease the flow of concrete, while narrower hoses may increase friction and clogging risk.	[75]

6.2 Extrudability

Extrudability refers to a material's ability to flow smoothly through an extruder or nozzle, which significantly impacts the printing process [76, 80]. A concrete mix with good extrudability provides consistent material flow, ensuring that printed layers are accurately formed. The material's flow is influenced by yield stress, which includes two components: static yield stress (the minimum stress required to initiate flow) and dynamic yield stress (the stress required to maintain flow) [26]. Importantly, yield stress changes over time, typically increasing as cement particles flocculate and an internal structure forms after mixing [81]. Therefore, understanding and controlling these properties is essential for successful 3DCP projects. Researchers have utilized various models to address the time-dependent behavior caused by cement hydration. The Mohr-Coulomb (M–C) model, as shown in Equation 4, has been widely applied for predicting early-age properties, such as modulus of elasticity and yield stress [82, 83]. However, this model often fails to accurately represent the nonlinear behavior of materials during early ages, with yield stress predictions exceeding actual test results by 20.6% to 46.0% [84]. Consequently, this raises questions about the utility of the M-C model for yield stress estimation. In contrast, the Drucker-Prager (D-P) model, represented by Equation 5, effectively characterizes yield stress and hardening stages, positioning it as a promising alternative. This model demonstrates good correlation with mechanical properties at early stages, with discrepancies in yield stress predictions varying from 3.3% to 7.1% [84]. Nevertheless, it still encounters challenges in simulating post-yield behavior. The yield criterion of the M-C model relies on cohesion (C) and the angle of internal friction (Φ), which are typically estimated through direct shear tests or triaxial testing. To improve accuracy, it has been suggested that the cohesion be adjusted to 0.75 times the test results when using the M-C model [84].

$$\tau = C + \sigma_n tan\emptyset ------(4)$$

$$F(I_1, J_2) = \alpha I_1 + \sqrt{J_2} - k = 0 ------(5)$$

In the above equations, τ is shear stress; σ_n is the normal stress; Φ is the internal friction angle; C is the cohesion; I_1 is the first invariant of the stress tensor; J_2 is the second invariant of the stress deviator tensor; k is the hardening function; and α is a frictional parameter. To effectively control the time-dependent behavior of materials, it is crucial to carefully select materials, proportion mixtures, and often incorporate specific admixtures to achieve desired extrudability. As concrete ages, the development of calcium silicate hydrate (C-S-H) at the contact points of cement grains results in a further increase in yield stress [81]. This duality presents a challenge: while low yield stress facilitates pumping and extrusion, it can also lead to shape loss. Conversely, high-yield stress concrete promotes shape retention and buildability but complicates pumping and extrusion processes due to increased viscosity.

The values of static and dynamic yield stress described in the literature for the various types of mortar paste are given below in Table 5.

Table 5 Static and dynamic yield stress values obtained by researchers for different types of printable concrete mix

Mix Type	Testing apparatus	Static yield stress (kPa)	Dynamic yield stress (kPa)	References
Cement-SCM blended mortar	Rotational rheometer	0.14-0.48	0.12-0.18	[44]
	Rotary rheometer		0.01-0.02	[85]
	Anton Paar MCR 302 rheometers	0.2−0.7	0.1	[86]
	-		0.1-0.2	[87]
	Rotation rheometer		1.2-1.8	[88]
	Vane shear test	0.3-0.9		[69]
		1.5-2.5		[89]
	ICAR rheometer	2.7-3.9		[90]
		1.9		[91]
		0.5-1.8		[92]
	Viskomat XL	3.3		[93]
	Anton Par MCR 102 rotational rheometers	3.2-6.8		[23]
Geopolymer mortar		0.4-1		[24]
	Rotational rheometer		0.09-0.3	[65]
Cement paste	Dynamic shear rheometer		0.1-0.3	[94]
	Rotation rheometer	0.2−0.7	0.5-0.6	[95]
			0.5-0.7	[96]
			0.6-0.7	[97]

Cement-based mortar	Anton Paar Rheolab rheometer	4	[98]

Researchers found that material compositions and admixture dosages greatly influence extrudability. For example, it is reported that the inclusion of larger-size aggregates reduces the yield stress and increases the plastic viscosity to a certain extent, while the addition of more fine materials reduces extrudability [24, 43]. The use of polycarboxylate-based superplasticizer (SP), a high-range water reducer, is preferred to improve workability [99]. However, when the SP dose increases, the initial static yield shear stress decreases. Additionally, mixes with high concentrations of sand can lead to blockage of the pipe during extrusion [24]. When yield stress goes beyond 0.9 kPa, mixes become difficult to extrude due to the structurization [69]. Extrusion of stiff mixes is complex and can rupture the filament while printing. More volume of voids is found in stiff mixes during extrusion, which affects the flexural strength of the printed structures [100]. Typically, extrudability tests rely on measuring extruder pressure or assessing the quality of the extruded strip. To achieve satisfactory extrudability, nozzle widths of 9 mm and 15 mm were used by Le et al. [69] and Lafhaj et al. [101], respectively, for the extrusion of 4500 mm and 500 mm long bands without breaking or clogging the nozzle (Fig. 11 a-b). Thus, balancing material composition, nozzle dimensions, and extrusion pressure is key to achieving smooth and consistent printing.

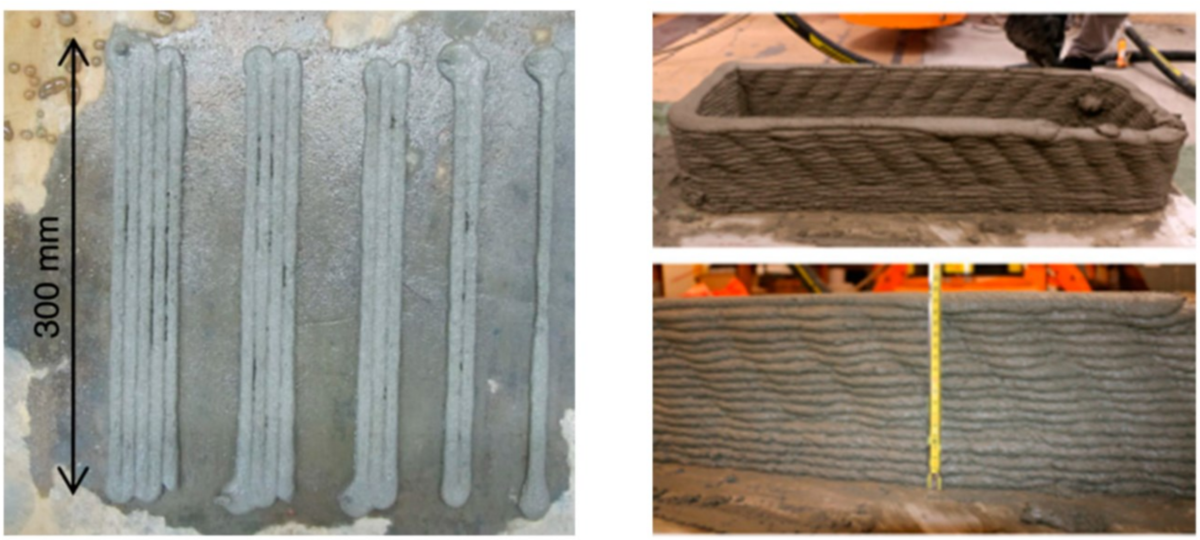

(a) (b)

Fig. 11 Samples prepared to evaluate extrudability (a) Extrusion of 4500 mm long band, (b) 20 layers of strip [69, 101]

6.3 Shape retention

Shape retention is an essential fresh property of 3D printable mixes. After coming out of the nozzle, the material must preserve its shape in accordance with the nozzle dimensions. This can be measured using a dimensionless value known as the shape retention factor (SRF).

$$\text{SRF} = \frac{\text{Cross sectional area of 3D printed sample before demoulding}}{\text{Cross sectional area of 3D printed sample after demoulding}} --- (6)$$

Materials with low slump value (high yield stress) are preferred to achieve a high shape retention factor (SRF), while those with low yield stress result in a low SRF [3, 24]. The height of each layer is checked for its shape retention capabilities after one hour of printing concrete [102]. Additionally, the printing speed also affects the shape retention capacity; with an increase in the printing speed, the width of the printed layer is reduced proportionally [103]. To further enhance the shape stability, nano-additives can be added to the mix [104]. Moreover, viscosity modifying agents (VMA), such as hydroxypropyl methylcellulose, are used as a thickening component in printed concrete to prevent segregation, increase thixotropy, and improve shape stability [8, 105]. The effects of different parameters, such as yield stress, VMA, and time, on shape retention are shown in Fig. 12.

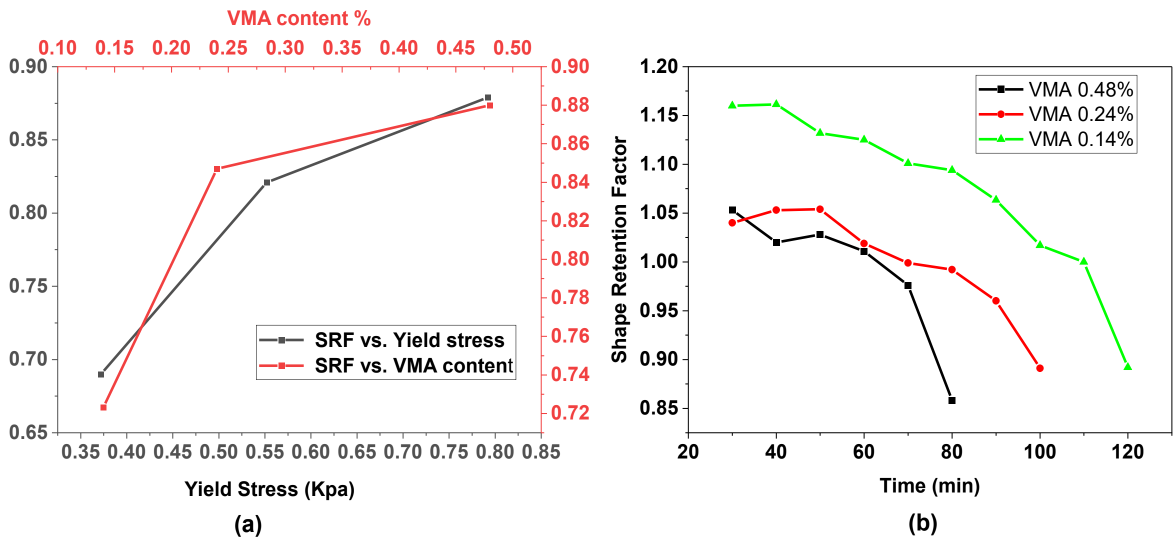

Fig. 12 Effects of (a) Yield stress [24] **and VMA** [105]**, (b) Varying percentages of VMA at different ages on shape retention ratio** [105]

Fig. 12(a) clearly shows that an increase in yield stress and VMA dosage leads to a corresponding rise in the shape retention factor (SRF). In contrast, Fig. 12(b) illustrates the variation of the SRF over time for different VMA percentages, revealing a consistent decline in SRF as time progresses after printing. Notably, while an initial increase in VMA dosage improves shape retention, a higher VMA concentration is associated with a gradual reduction in SRF over time. This suggests that although VMAs enhance the material's thixotropy and immediate shape stability, their prolonged effects on shape retention diminish as time elapses after printing.

6.4 Open time

The open time is the length of time from the moment dry concrete mix first comes into contact with water until the material is acceptable for printing. For adequate extrudability, flowability, and interlayer bond strength, a long open time is necessary but it should not exceed 90 minutes after water-cement contact [69]. The recommended working duration for concrete mixtures used in 3D printing is between 50 and 80 minutes [106]. Open time can be decreased by increasing the dosages of viscosity-modifying agents (VMA). Chen et al. found the optimal dosage of VMA for printable concrete to be 0.24%. [105]. Additionally, Panda et al. [24] found that replacing 5-15% fly ash with GGBS instead of using an accelerator/retarder could vary the open time, leading to great shape-retention abilities.

6.5 Buildability

It refers to the ability of layers to withstand the pressure and weight of layers above them without deforming or failing structurally (Fig. 13).

Fig. 13 (a) Buildable concrete **(b) Failed in buildability** [107]

Fig. 13 (a) shows how the lower layer can support the upper layer steadily, while Fig. 13 (b) displays the contrast. The thixotropy of the material used in 3DCP affects its buildability and yield strength [23]. Incorporating nano clay enhances these properties, leading to improved thixotropy, yield potential, and subsequently, higher buildability and shape stability [23, 108]. However, exceeding the minimum thixotropy value can lead to high extrusion pressure and lower interfacial bond strength if not tailored to the part design. For instance, due to higher thixotropy and yield stress, the buildability of the modified mix (OPC+ fly-ash + silica fume + nano clay) is seen to be two times higher than the control mix (OPC + fly-ash + silica fume) [23].

Standoff distance (SD) (distance between the surface of the previously deposited layer and the tip of the nozzle) affects interlayer strength. While high-yield stress materials increase buildability, if the standard deviation (SD) of the printed material is equal to the nozzle width, it can result in weaker interfaces [23, 81]. Reducing the standoff distance can significantly enhance interface strength, thereby improving the structural integrity of the printed object.

Furthermore, materials with lower thixotropy and yield stress can be effective for 3DCP, contributing to smoother extrusion and improved interlayer adhesion. A combination of nano clay and PCE-based superplasticizer is recommended to balance the trade-off between buildability and bond strength [23]. Therefore, researchers must carefully balance material properties, printing parameters, and buildability considerations to achieve the desired structural integrity and quality in 3D-printed objects.

6.6 Shrinkage behavior

The absence of formwork in 3D-printed concrete creates additional shrinkage; thus, the risk of crack formation increases. These cracks create pathways for chemical compounds to enter the printed element, reducing its durability. In conventional concrete, the three primary shrinkages are plastic, autogenous shrinkage, and drying [109]. Due to the evaporation of water that has been present on the surfaces in its fresh state, plastic shrinkage develops when the concrete is in the plastic condition. In contrast, due to low water-to-cement ratios, autogenous shrinkage happens when there is not enough water available for the process of hydration in mixtures [110]. In 3DPC, due to the lack of formwork and reduced water-binder ratios (w/b ratio < 0.30), the material may be more prone to both plastic and autogenous shrinkage [110]. Drying shrinkage, on the other hand, occurs in a hardened concrete mixture where more water is present than necessary for the hydration process because of the high water-cement ratio. Table 6 discusses the types of shrinkage, their cause, and their effects on the concrete 3D printing.

Cracks formed because of plastic shrinkage are shown in Fig. 14. These cracks are unappealing, can cause corrosion in steel reinforcement used in 3DCP, and if 3D printed concrete is unreinforced, reduces the tensile capacity. Further, it also makes 3DPC susceptible to carbonation.

Table 6 Shrinkage behavior of 3D printed concrete

Type of shrinkage	Cause of increases/decreases in shrinkage	Effects on 3D-printed concrete	Methods adopted to measure the shrinkage	Ref.
Plastic shrinkage cracking (PSC)	High surface area to volume ratio	Excessive pore water evaporation causes plastic shrinkage deformation	ASTM C1579 test method or shrinkage rig method	[111]
	Lack of formwork	Initiate the corrosion of steel reinforcement, increases carbonation, and can reduce tensile capacity if 3DPC is unreinforced	BS EN 12617-4:2002,	[3, 5]
Drying shrinkage	Increasing sand/cement ratio from 0.8-1.0 at different environmental conditions	10% reduction in drying shrinkage for both traditional and 3DPC	BS EN 12617-4: 2002, and ASTM C596-07	[112]
	At fixed (24°C and 50% RH) condition	Drying shrinkage reduced by 25–30% compared to traditional casting		[112]
	Rise in temperature from 24 to 35 °C	At constant humidity between 45-50%, the increase in temperature has a minor effect on drying shrinkage		[112]
	In tropical weather curing environment (35 °C and 85 percent RH)	Shrinkage deformation dropped nearly 2.5 times		[112]
Carbonation shrinkage	Increase in mass with increase in drying shrinkage	3D-printed concrete is susceptible to carbonation shrinkage	Treatment with phenolphthalein	[112]

Early age shrinkage	Interlayer slip	Adversely affect the durability and long-term interlayer bond strength of 3D-printed concrete	LVDT sensor	[113]
Plastic and dry shrinkage	Absence of coarse aggregate	Aggregate to binder ratio of roughly 1.3–1.6 in 3DPC accelerate the shrinkage process	DIC technique following UNI/EN 1339 (2003)	[19]
Autogenous shrinkage	Use of superabsorbent polymers (SAPs)	Enhance moisture content and reduced porosity results in the reduction of autogenous shrinkage by 200%, Interlayer bond strength reduced	Digital dilatometers according to ASTM C1698	[114]
	At a low water-cement ratio (0.2-0.4)	Shrinkage is in the range of 330 to 850 µm/m for high-performance concrete, which has properties similar to 3DCP	Modified ASTM C1581, Eddy-current displacement sensor (ECDS), ASTM C 1698-09, AGS test	[28, 115]
Total shrinkage	At water cement ratio between 0.25-0.36	Shrinkage value is ≤ 800 µm/m for high-performance concrete made up by using fly-ash, GGBS, recycled aggregate	Chinese standard GB/T 50082-2009, ASTM C157	[116, 117]
	Mortars with deficiency of coarse aggregate and compressive strengths of more than 50 MPa	Shrinkage is approx. 1200 µm/m	ASTM C157, JC/T 603-2004, to ASTM C596-2001	[118]
	Addition of 4% admixture	Shrinkage can be reduced by roughly 23 percent	Leaser measurement sensor (sensor pick the light reflected from steel reference	[119]

			points fitted at both the end of the prepared sample)	
	External curing	Reduced shrinkage from 5178 to 1031 µm/m but not suitable for industrial use because the curing procedure inhibits the printing of consecutive layers during continuous printing; hence internal curing is more beneficial		[119]

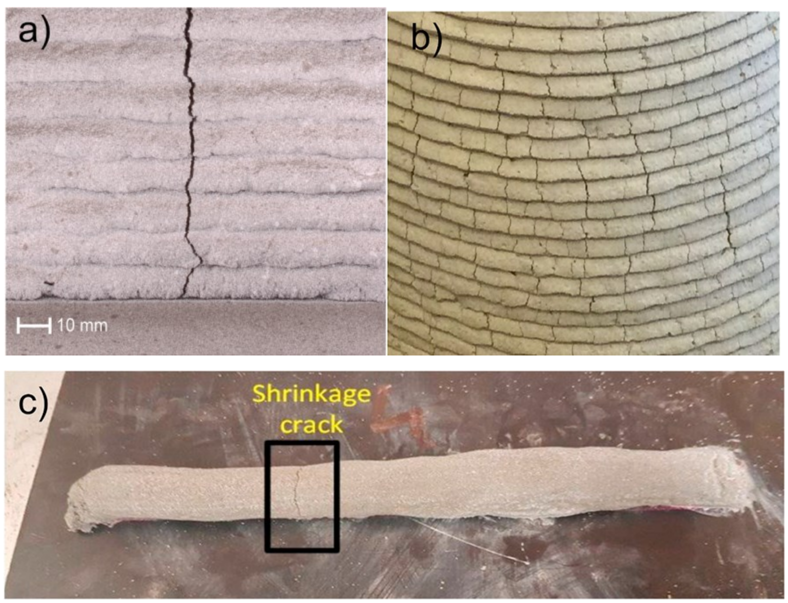

Fig. 14 a) Exposure for the first 2 hours after printing in moderate evaporation rate [113], **b) Excessive crack formation due to early age shrinkage** [3], **c) Crack after 1 day of curing at laboratory temperature** [120]

However, limited findings related to shrinkage are available, and many researchers have highlighted the issue of total shrinkage in printed concrete as a scope of future research.

7 Engineering properties of 3D-printed concrete

Numerous variables, including layer orientation, interlayer gap time, and the direction of loading, have an impact on the compressive, flexural, and splitting tensile strength of 3D-printed concrete [98]. Some other studies [30, 121] have shown that directional dependency is seen in both compression and flexural strengths. Researchers have employed various specimen sizes, typically saw-cut from printed slabs, to account for this. Compression tests, following NEN-EN 12390-3, were performed on specimens' sizes 70.7 × 70.7 × 70.7 mm³ [122], 50 × 50 × 50 [123], and 40 × 40 × 40 mm³ [124]. Three-point bending tests following NEN-EN 196-1 were used to determine the flexural strength. The specimen sizes adopted by researchers are 90 × 90 × 360 mm³ [122] and 40 × 40 × 160 mm³ [123, 124]. Additionally, the tensile splitting test was performed on the cube specimens of sizes 40 × 40 × 100 mm³ [124], 70.7 × 70.7 × 70.7

mm³ [122], 40 x 40 x 40 mm, according to the NEN-EN 12390-6. Fig. 15 shows the variations in layer orientations and loading directions used during testing.

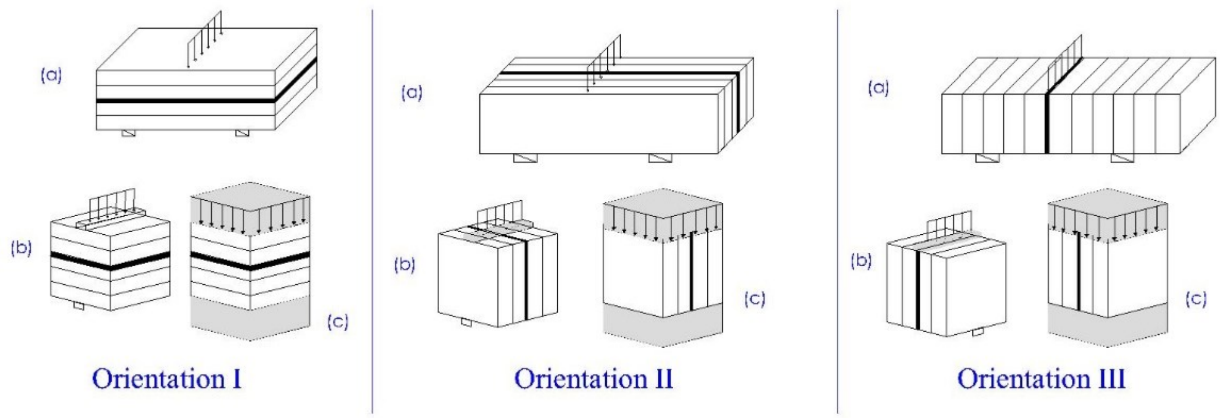

Fig. 15 (a) Flexural test, (b) Splitting tensile test, and (c) compression test in the different orientations of the 3D printed layer [125]

7.1 Effects of layer orientation on the strength properties of 3D printed concrete

Strength properties are greatly impacted by the anisotropy of the printing process, particularly in regard to interlayer bonding. The variation in compressive, flexural, and split tensile strength across different layers is depicted in Fig. 16 and is discussed in more detail below.

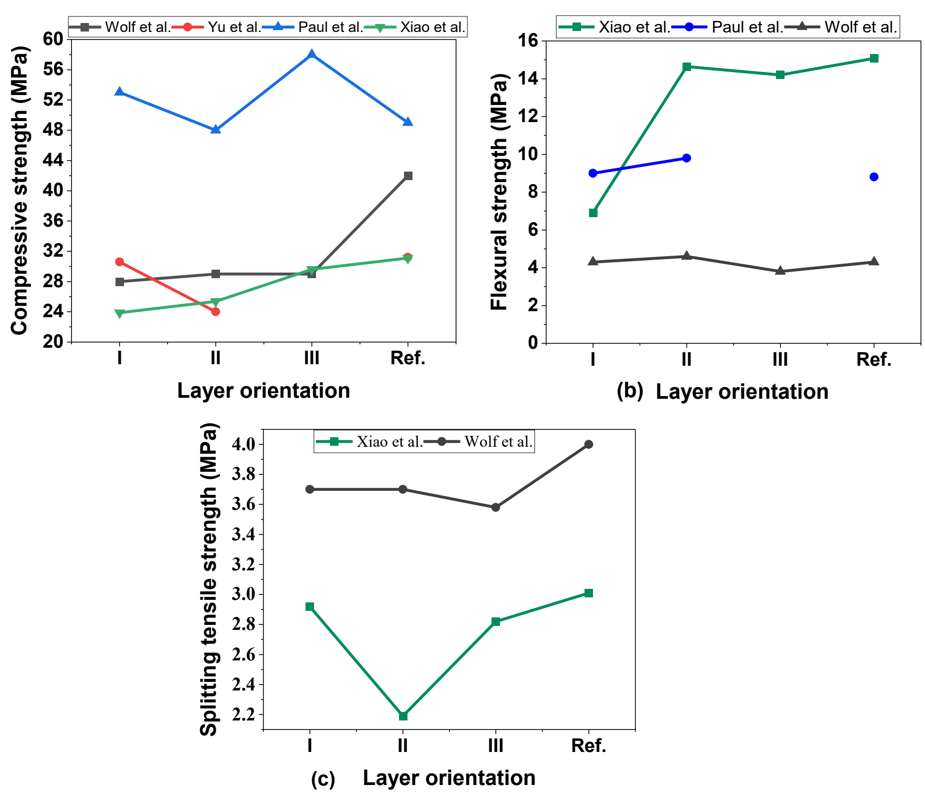

Fig. 16 Effects of layer orientation on (a) Compressive, (b) Flexural, [148], and (c) Splitting tensile strength [31, 122, 123, 125]

In the compressive strength test, orientations II and III (Fig. 16) were combined due to equal loading. Specimens printed in orientation III exhibited a 15% higher compressive strength than conventionally cast specimens at 28 days [24]. However, Yu et al. [123] noted that conventionally cast specimens had nearly equal strengths when the interface layer was perpendicular to the loading direction. For flexural strength, control samples were lower than those printed in orientations I and II by 6% and 12%, respectively [26]. Conversely, Wolf et al. found flexural strength in orientation III to be 14% lower than in the other orientations [125]. Compared to the 50% differences reported by Le et al. [98] and Panda et al. [124], this reduction is negligible.

These differences stem from anisotropy due to the printing process, with strength influenced by interlayer bond strength under loading conditions. The splitting tensile test revealed higher strengths in control specimens than printed specimens, regardless of loading direction [122, 126] (Fig. 16c). Compression and flexural strength were lowest in the orientation I while splitting tensile strength was lowest in orientation II [122]. However, Wolf et al. [125] found less significance in directional dependency. The anisotropic strength in flexural and splitting tests improved with 100% recycled fine aggregate and 1% fiber content; it decreased without fiber. This examination underscores the complexity of determining the mechanical characteristics of 3D-printed concrete, emphasizing the importance of orientation, loading direction, and interlayer bonding [122].

7.2 Effect of interlayer gap time on the strength properties of 3D printed concrete

The flexural and tensile strength of interlayers decreases as the printing interval increases, primarily due to poor adhesion caused by drying surfaces from larger interlayer gaps [98, 124]. Increased print head speed and nozzle height lead to micro voids, reducing interfacial tensile strength [25]. For optimal layer bonding in the 3DCP, it's crucial to minimize interlayer gap durations and maintain a gradual construction rate to ensure materials gain adequate stiffness [127]. As shown in Figs. 17, 18, and 19, interlayer gap periods and loading orientations significantly affect the compressive, flexural, and splitting strengths.

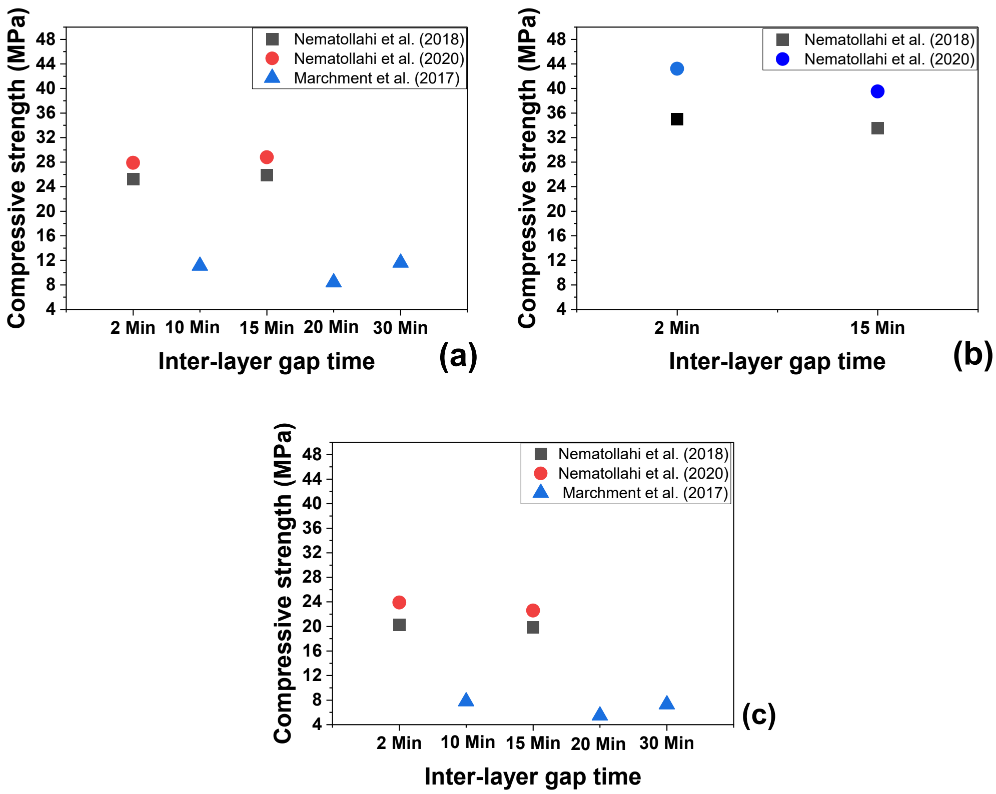

Fig. 17 Effect of interlayer gap time on the compressive strength in (a) perpendicular, (b) Longitudinal, and (c) lateral directions [127–129]

In a study by Nematollahi et al. [127, 129], a 3D printable geopolymer one-part mix formulation was created using only water and a solid activator. The compressive strength was highest in the longitudinal direction and lowest laterally, with the perpendicular direction exhibiting 24–30% higher strength than lateral, attributed to stronger interlayer bonds. Interestingly, compressive strength at 2 and 15-minute intervals were similar, suggesting that interlayer gap time has minimal impact within open time [127, 129].

The impact of interlayer gap time on the flexural strength of 3D printed concrete when loading was in perpendicular, and lateral directions are shown in Fig. 18. Notably, flexural strength is significantly greater in the perpendicular direction—51–65% higher, depending on the interval. Samples with a 2-minute gap time displayed 6-17% higher flexural strength compared to those with a 15-minute gap, indicating a strong influence of interlayer gap time on 3D-printed concrete properties [129]. Wolfs et al. [125] reported a 16% reduction in flexural strength at 24-hour intervals compared to 15-second intervals and a 21% decrease in splitting tensile strength. This reduction is linked to interface dehydration during extended intervals. However, for interlayer gap times of 1 hour and 4 hours, strength reduction remains insignificant, indicating adequate specimen coverage during extended printing delays [125].

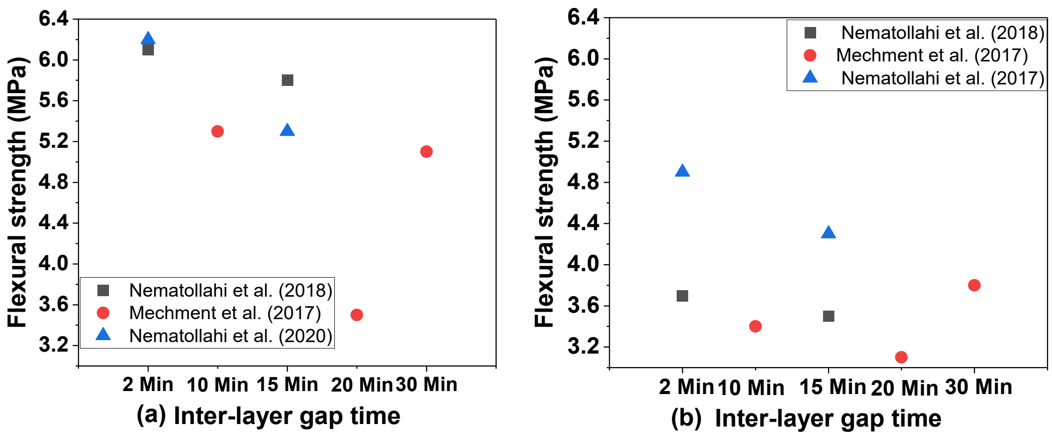

Fig. 18 Effect of interlayer gap time on the flexural strength in (a) perpendicular, (b) lateral direction of loading [127–129]

In addition, the nozzle height effect on flexural strength is also being studied by the researcher, and the results are shown in Fig. 19(b). There is no obvious relationship between nozzle height and specimen strength at both 15-second and 24-hour interlayer time intervals.

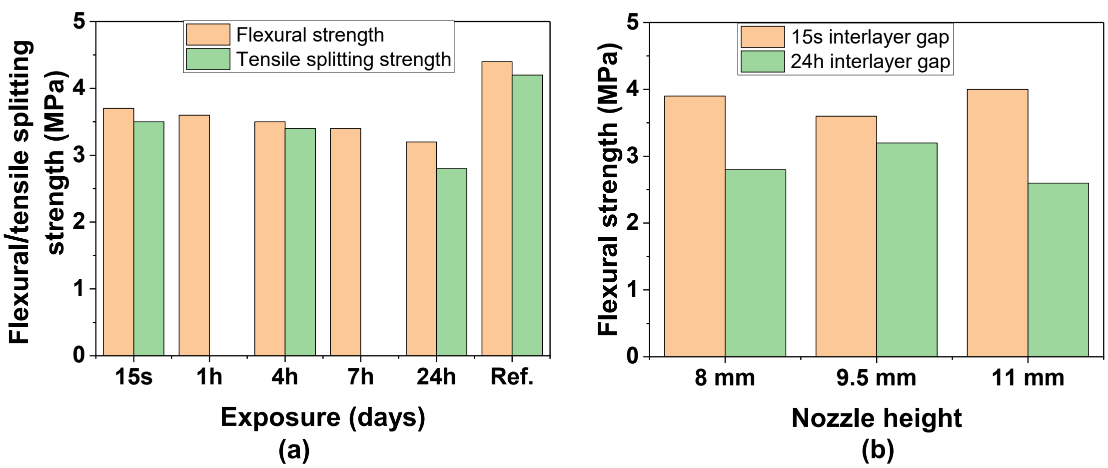

Fig. 19 Flexural and splitting tensile strength (a) effect of interlayer gap time (b) Impact of interlayer gap time of 15s and 24h on 3 different nozzle heights [125]

The effect of dehydration on the exposed and covered interface between interlayer gap times was studied, particularly in relation to flexural strength, as illustrated in Fig. 20 [125].

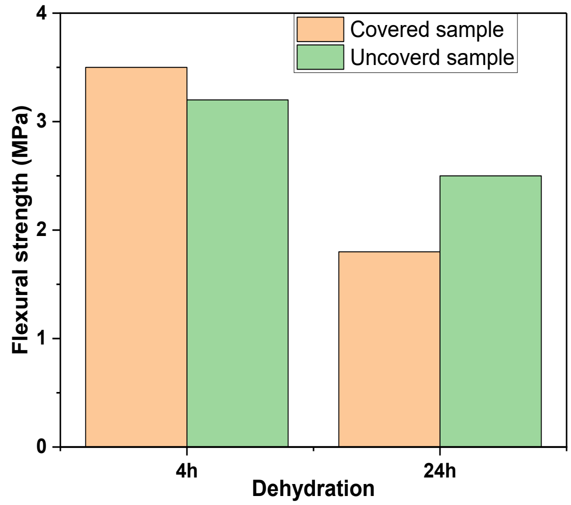

Fig. 20 Effect of dehydration on flexural strength for covered and uncovered samples for gap periods of 4 hours and 24 hours [125]

It was observed that strength drops are greater for uncovered specimens when comparing printed specimens with and without covers at the same interlayer gap time. A higher drop was anticipated because the 24-hour samples were exposed for a longer duration than the 4-hour specimens, allowing for more dehydration [130].

7.3 Effect of fiber content on the strength properties of 3D printed concrete

The effect of different types of fiber, such as polyethylene fiber and polyvinyl alcohol fiber, on the compressive, flexural, and split tensile strength of mould-cast and 3D-printed concrete is shown in Fig. 21, 22, and 23.

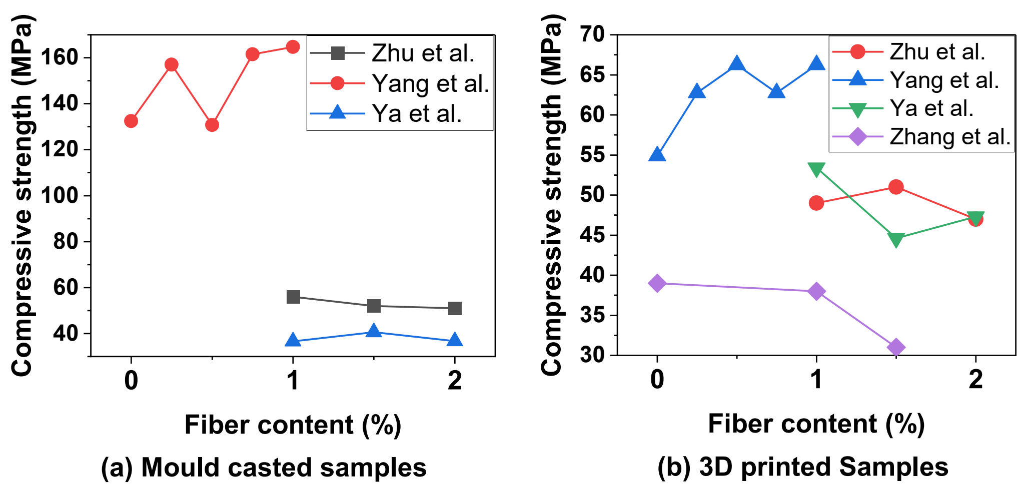

Fig. 21 Effect of fiber content on the compressive strength in (a) Mould-cast sample, (b) 3D printed sample [131–134]

The mould-cast specimens yielded 2-12% higher compressive strength than the printed samples, depending on the fiber percentages (Fig. 21) [132, 133]. The lower compressive strength of specimens of 3D-printed concrete may be caused by pores present in the printed layers [132]. The above statement contradicts Ye et al. [131] findings, where no matter how much polyethylene fiber is in the specimens, the obtained compressive strength is higher than that of cast specimens. However, according to Zhang et al. [134], the compressive and flexural strengths of the printed specimen were found to be reduced by the excess polyvinyl alcohol fiber (PVA).

Figs. 22 (a) and (b) demonstrate how fiber volume significantly affects the flexural strength of both cast and printed specimens.

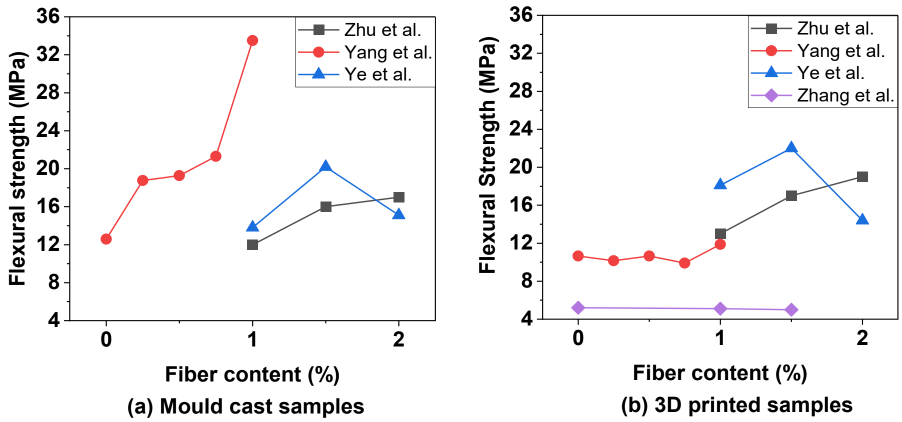

Fig. 22 Effect of fiber content on the flexural strength in (a) Mould-cast sample, (b) 3D printed sample [131–134]

The flexural strength of cast specimens was observed to be higher than printed specimens, similar to compressive strength (as shown in Figs. 22). However, when fibers are mixed, an increase in fiber content results in specimens that are stronger when cast in a mould. Notably, the flexural strength of 3D-printed specimens at 1.5% fiber content exceeds that of mould-cast specimens [131, 133]. This increase in strength can be attributed to the higher fiber concentration along the printing direction. For both mould-cast and printed specimens, the splitting tensile strength first increased as the fiber content increased (up to 1.5%), and then it decreased at 2% (Fig. 23). The lower value of strength at 2% fiber content is due to the high average crack width [124]. Despite this, mould-cast samples have a higher overall splitting tensile strength than 3D-printed specimens [131]. Nevertheless, Yang et al. [103] discovered that the addition of fiber to the mixture increased the splitting tensile strength of 3D-printed specimens 1.3 times over mould-cast specimens.

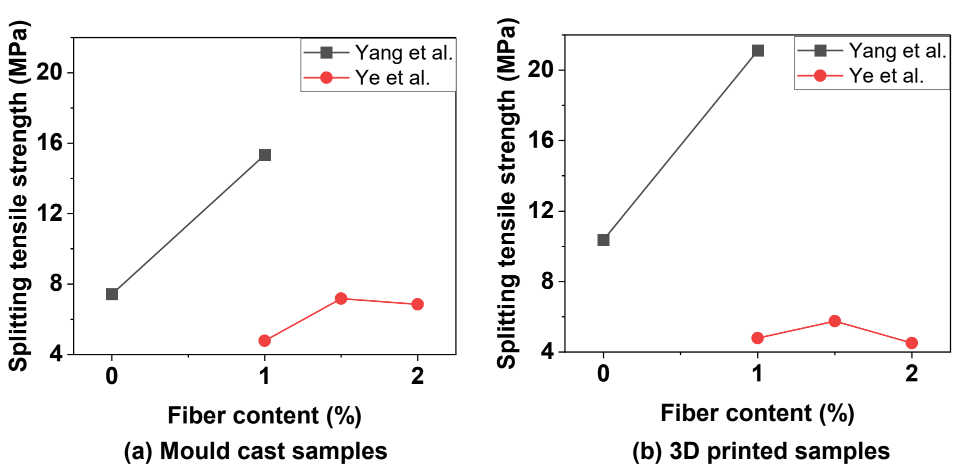

Fig. 23 Effect of fiber content on the splitting tensile strength in (a) Mould-cast sample, (b) 3D printed sample [131–134]

8 Durability

8.1 Sulfuric acid attack

Surface deterioration of concrete specimens exposed to 1% and 3% sulfuric acid solutions at different ages are shown in Fig. 24 and Fig. 25, respectively [135].

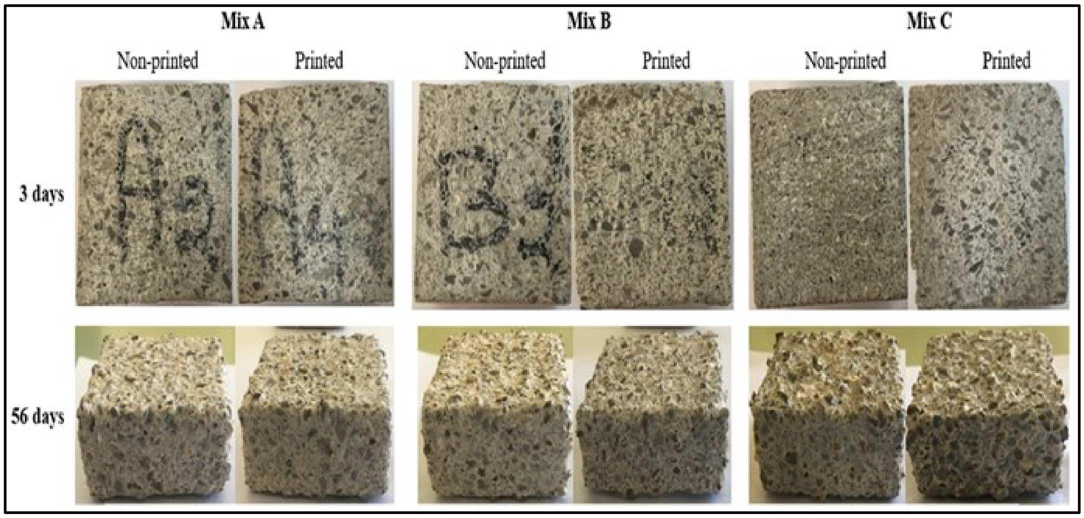

Fig. 24 Progressive degradation of printed and non-printed samples in 1% acidic solution [135]

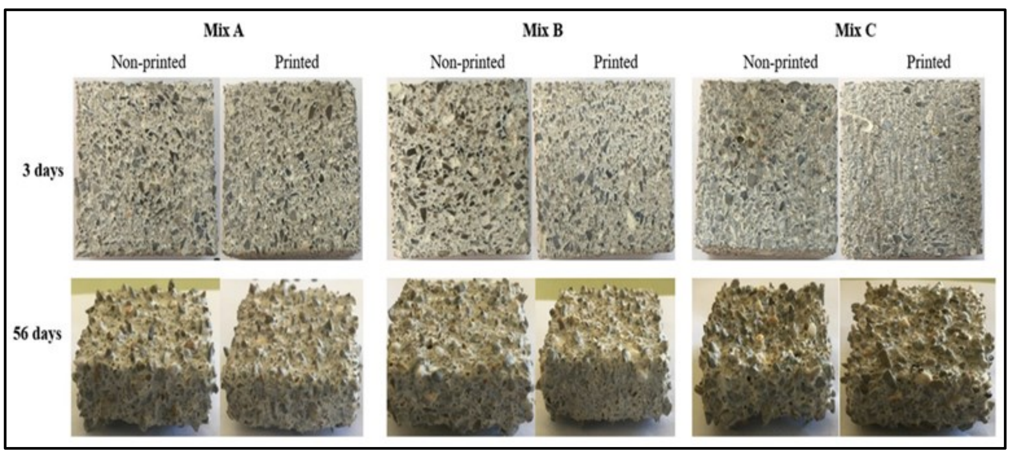

Fig. 25 Progressive degradation of printed and non-printed samples in 3% acidic solution [135]

The specimens were submerged in 98% concentrated H_2SO_4, and the volume of the solution was established at four times that of the submerged specimen in accordance with the standard test procedure (ASTM C1012/C1012M - 18b). To stop evaporation, specimens were put on plastic supports inside of sealed containers. The solution was changed after 3, 7, 14, 21, 28, and 42 days, and the storage temperature was kept constant at 22±2 °C.

The degradation rates were the same for the printed and non-printed samples of all mixtures [135]. On the contrary, according to Zhang et al. [136], where specimens were immersed in a 5% Na_2SO_4, 3DPC exhibited greater resistance to sulfate attack than mould-cast concrete. Mould-cast specimens started reducing their strength at 30 cycles of alternate wet and dry (duration of each cycle is 24 hours), while 3D-printed specimens started deteriorating from 90 cycles. Fig. 26 explains the mass loss of printed and non-printed concrete samples due to sulfuric acid solutions.

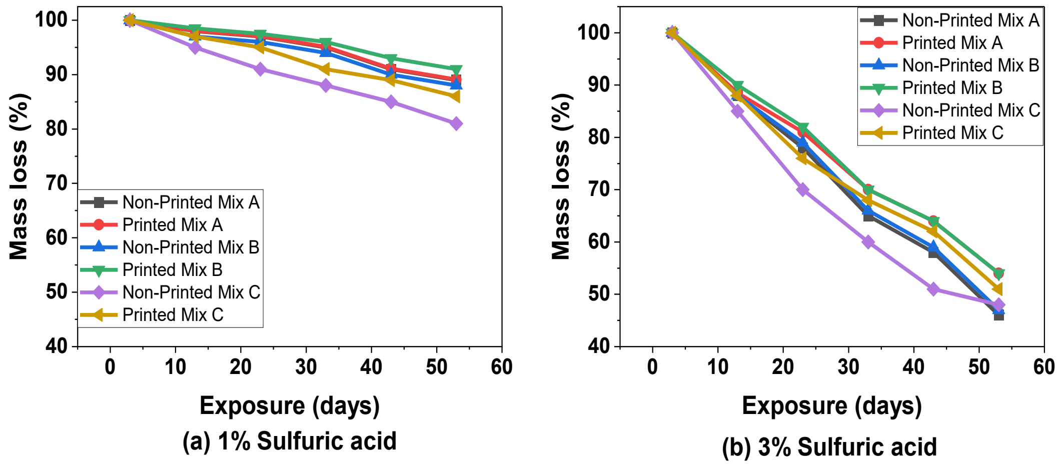

Fig. 26 Mass loss of printed and non-printed concrete samples subjected to solutions containing (a) 1% and (b) 3% sulfuric acid [135]

The mass loss of specimens associated with 1% sulfuric acid exposure is significantly lower than that of the specimens immersed in a 3% sulfuric acid solution. However, the declination rate in non-printed samples is substantially greater than the declination rate in printed samples. This can be attributed to more accessible pores present and also due to exposing a larger portion of the paste surface [135]. The 3D-printed element is strong enough to withstand additional damage and mass loss [135]. This indicates that the interlayers are preventing the solution from entering the element further, which causes it to react and destroy a larger area of the specimen surface. It is significant to note that neither a failure of printed specimens nor the development of cracks along that plane occurred in the interlayer region.

8.2 Chloride attack

Ingress of chloride ions is higher in printed concrete than in casted concrete. The depth of the chloride attack went up in harmony with the time gap between layers [137]. The variation of chloride depth with interlayer gap time is given in Table 7.

Table 7 Variation of chloride penetration with interlayer time gap

Sl. No.	Interlayer gap time (min)	Chloride penetration	References
1.	10	40.86 mm	[22]
	20	65.90 mm	
	30	78.16 mm	
2.	0	40%	[138]
	10	30%	
	60	60%	
3.	0	31%	[139]
	30	54%	

It has been observed that the chloride penetration depth increases with the increase in the interlayer gap time. Layer tearing creates pathways for chloride ingress, which may aid in the onset of corrosion [22]. The rough and porous nature of 3DPC is responsible for the outer layer capillary water absorption, which is seen to be comparatively more than the inner bulk material [137]. Chloride penetration in 3DPC specimens shows that penetration for interval periods of 24 hours is much greater than interval times of 2 min. This is due to the fact that at 24-hour intervals, surface moisture between layers evaporates [140]. Consequently, more pores and micro-cracks were developed, which resulted in a lack of fusion between layers [141]. Neutron radiography showed that water sorption in concrete printed with a 15-second interval varied with print speed, with higher speeds resulting in lower water sorptivity without preferential water infiltration at the interlayer [138]. Further, the rapid chloride migration test showed a lower rapid chloride migration coefficient (D_{RCM}) for mould-cast than 3D-printed concrete (Fig. 27). The lower migration coefficient in a 3D-printed specimen is due to the existence of deeper migration zones between the adjacent layers through which chloride ions move deeper and more rapidly through the interconnected voids between the filaments in these regions [136]

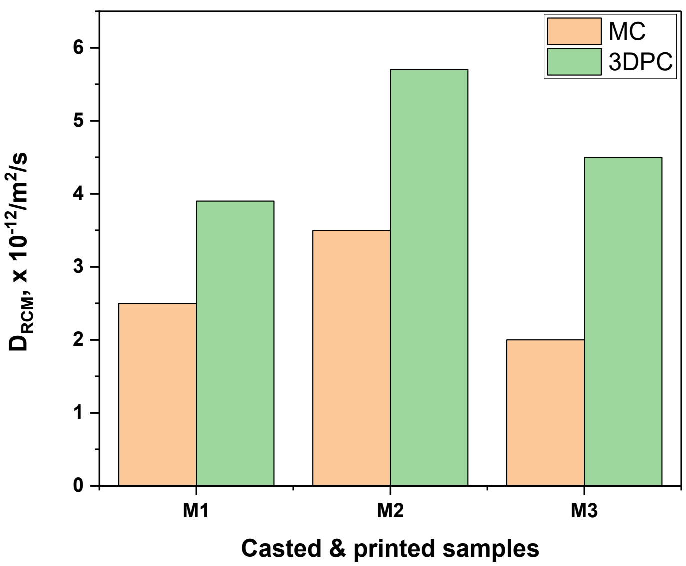

Fig. 27 Chloride migration coefficient for mould-cast and 3DPC specimens [136]

8.3 Freeze-thaw attack

The increased cycle of freeze-thaw reduced the dynamic modulus of elasticity of concrete. 3DPC specimens had a lower dynamic modulus of elasticity than mould-cast specimens after 200 cycles [136]. However, the weight loss was higher in mould-cast specimens. This is primarily due to the fact that moisture in the interlayer gaps is consistently oxidized from the interior of the 3D printed specimen during the freeze-thaw cycle, leading to less dynamic modulus of elasticity than the mould-casted specimen [136].

A significant change in compressive and flexural strength was not observed up to 50 freeze-thaw cycles; in fact, after 50 freeze-thaw cycles, the decrement in flexural strength was only 9–21% for different samples as compared to their initial strength. The associated resistance to freeze-thaw action is possibly attributed to the homogeneous and dense microstructure [142]. Additionally, air-entraining additives are often used in cold areas to enhance the material's resistance to freeze-thaw attacks. While interlayer bond strength is considered more critical than other mechanical characteristics, the presence of air-entraining compounds creates additional voids that contribute to better frost resistance [143]. Furthermore, pumping concrete is found to lower the void size and spacing, thereby making the concrete withstand freeze and thaw attacks [143].

8.4 Carbonation

The variation of carbonation depth with age in mould-cast and 3D-printed concrete is shown in Fig. 28.

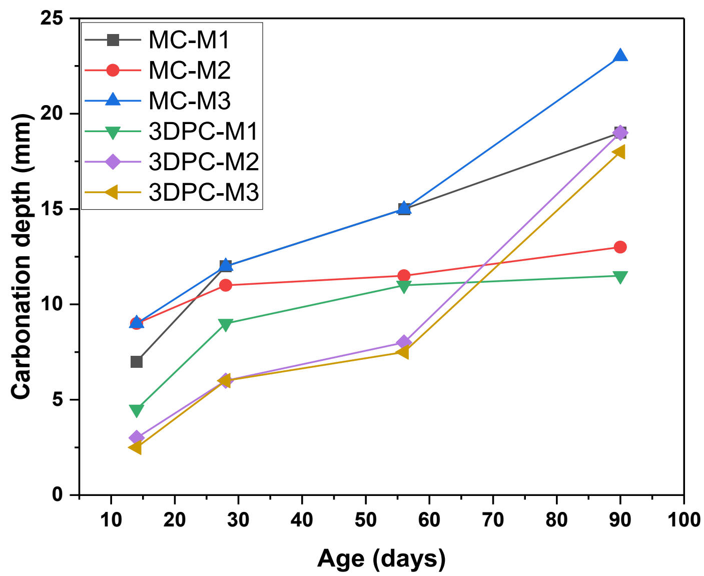

Fig. 28 Variation of carbonation depth with the age of mould-cast and 3DPC specimens [136]

The carbonation depth of 3DPC is less than the mould-cast specimen and increased over time [136]. According to Sanchez et al. [144]**,** the 3DPC showed a nonuniform and faster carbonation rate due to the interlayer interfaces. The development and advancement of microstructural inhomogeneities in 3DPC with regard to carbonation, especially with regard to capillary porosity at layer interfaces, are thought to require thorough research. Lower carbonation depths in cast specimens than in 3DCP specimens are ascribed to the interconnected pores in the interlayer regions (IRs) and critical layers of the 3DPC specimens [22]. Due to the absence of fusion generated by the gap time at the critical layer, the carbonation depth increased as the gap time increased. Carbon dioxide (CO_2) first penetrated the critical layer, followed by penetration above and below the critical layer through the matrix.

9 Microstructural analyses

Mechanical testing is supplemented by SEM studies in the micrometer (μm) range by Nerella et al. [126] and SEM images of two mixes C1 (cement + sand + water + superplasticizer) and C2 (cement + micro silica suspension + fly ash+ sand + water + superplasticizer) as shown in Fig. 29. Higher porosity at the interface of two layers in mix C1 (Fig. 29). Microstructural analysis of mix C1 at 1 min and 1-day time gap with 1 mm and 500 μm scale, respectively is shown in Fig. 29. Weak interfaces and extensive voids detected in microscopic images at the age of one day indicates the associated reason for a drastic reduction in flexural strengths. However, long separation zones between layers seen at the age of one day appeared to have already healed with a filler substance developed at the interface, which was misleading.

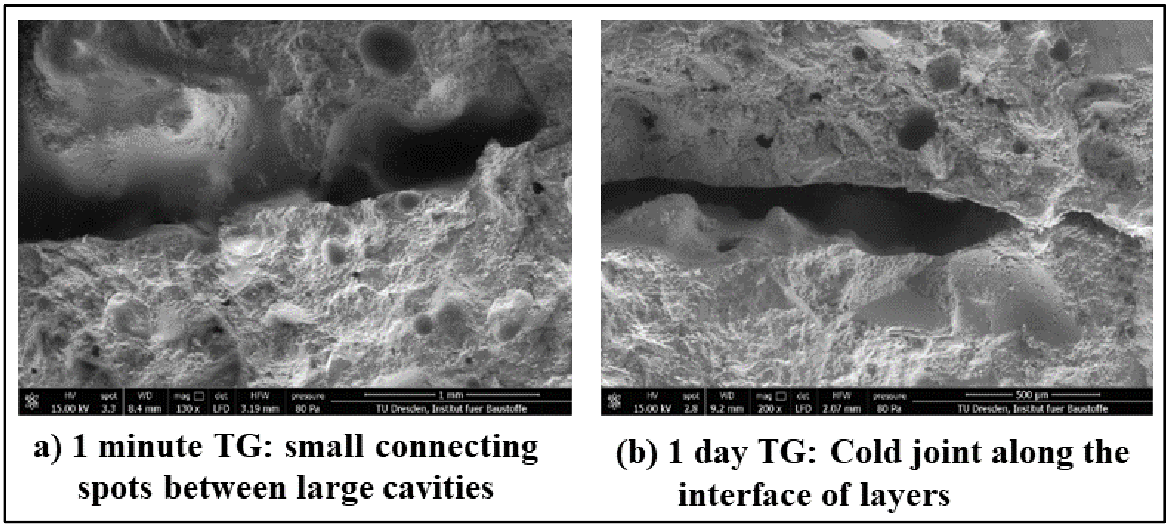

Fig. 29 SEM images for concrete C1 at an age of 1 day obtained for specimens produced with different time gaps (TG) [126]

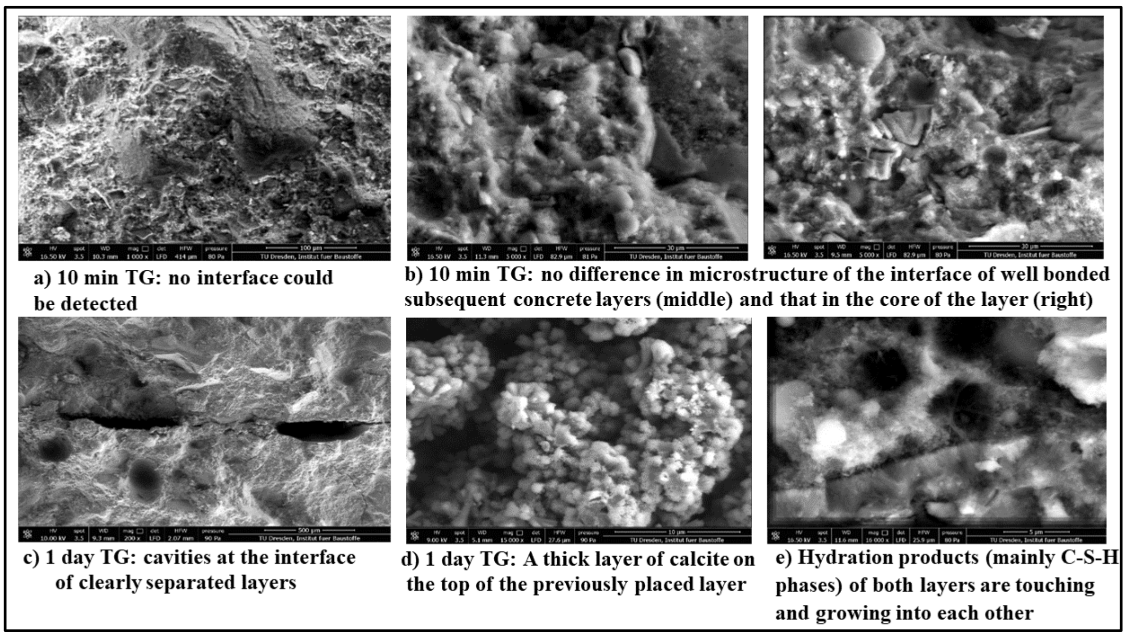

Fig. 30 SEM images for concrete C2 at the age of 1 day obtained for specimens printed with different time gaps (TG) [126]

The SEM measurements indicate that larger gap times produce more distinct interfaces between layers. Specimen C2, which underwent carbonation with a 1-day gap, shows a clear calcite phase formation on the top surface of the prior layer, hindering strong bonding with the second layer (Fig. 30(d), 10 µm scale). In contrast, specimens printed with shorter gap times, such as one minute, exhibit ettringite, calcite, and/or portlandite phases instead of the C-S-H phase at the core or interface (Fig. 30(e), 5 µm scale). Mechanical test results support this observation (Fig. 17(c)). An optical microscope investigation of the cracked surfaces of covered versus exposed specimens with a 4-hour interlayer gap reveals that dehydration affects hardened properties. Exposed samples display a smoother crack surface and higher void content compared to protected specimens with the same interlayer lengths (Fig. 31) [125].

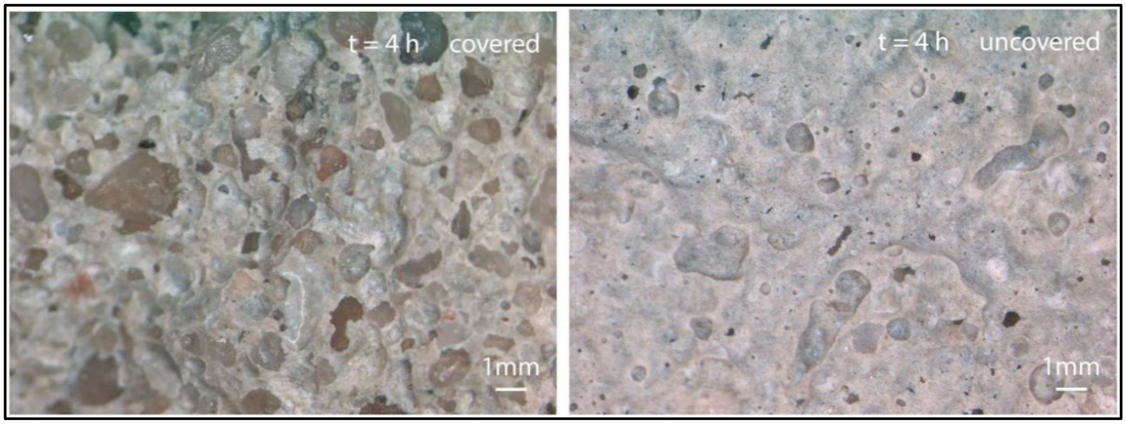

Fig. 31 Optical microscope images of the crack surfaces of covered (left) and exposed (right) specimens taken over a 4-hour interlayer gap time [125]

A microstructural study conducted on the lightweight engineered cement composite prepared to utilize hollow glass microspheres (HGM) named iM16K and S38HS as lightweight ingredients, and PVA fibers showed fully oriented fibers (Fig. 32). Bridging effect offered by fibers that stop the extension of macro-crack as well as initiation of micro-crack was also noticed [145]. Further, it also helped increase toughness and the ability to absorb energy.

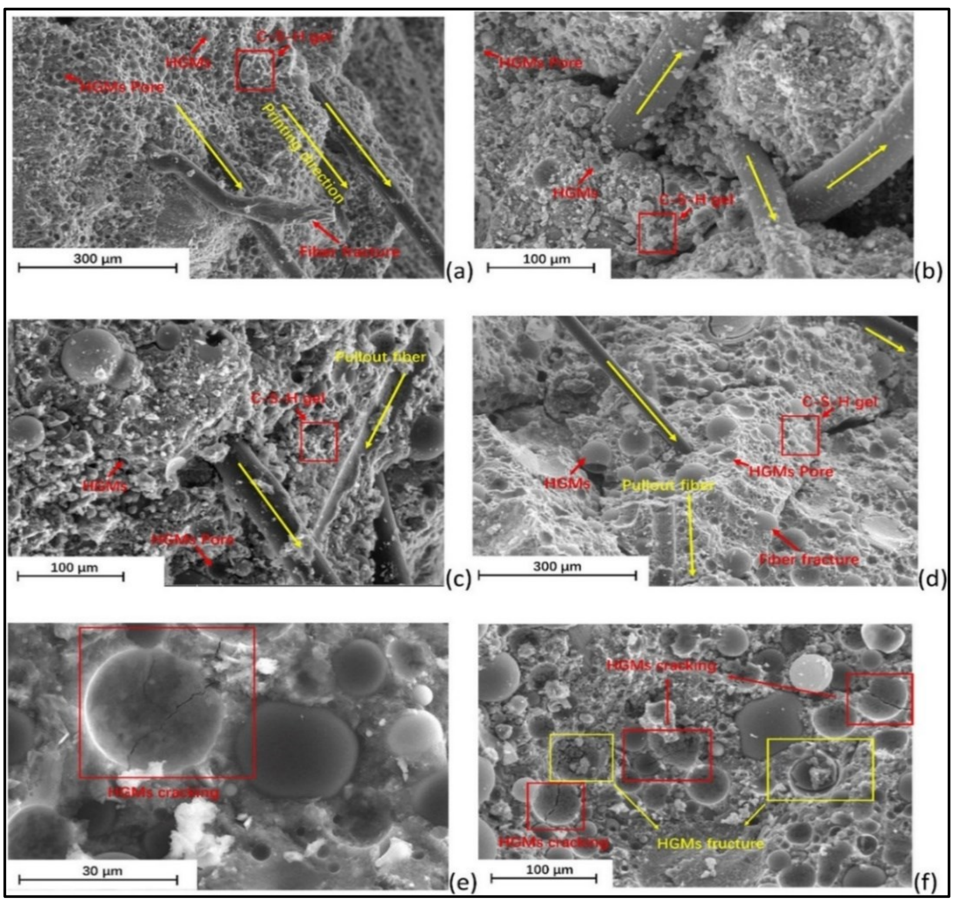

Fig. 32 SEM images of lightweight engineered cementitious composites, iM16K as lightweight ingredients (a) printed M60, cast (b) M60, (c) M100, (d) S60, (e) S80, and (f) S100 [145]

10 Advanced strategies in 3DCP

As 3DCP evolves, several advanced strategies have emerged that push the boundaries of traditional construction methods. These strategies include the incorporation of specialized binders, recycled aggregates, lightweight aggregates, and the use of reinforcement, all of which play a critical role in enhancing both the sustainability and structural performance of 3D-printed concrete structures. This section explores these advancements, demonstrating how they contribute to the next generation of 3DCP technology by improving material efficiency, strength properties, and environmental impact.

10.1 Sustainable and functional printable concrete materials

10.1.1 Alternative binder system

To develop a suitable mortar for 3D printing, high-volume fly ash mixed with cement is recommended due to the thixotropic properties of Portland cement [146]. The addition of calcined clays, especially those with varied metakaolin contents, can significantly enhance rheological properties such as flow consistency and buildability while accelerating hydration and early-age strength development [147]. This enhancement is due to the small grain size and high specific surface area of calcined clays, which improve particle packing and structure formation in mixtures. However, a high air void content at the interface can compromise interlayer adhesion, particularly in systems with higher metakaolin proportions [147]. Replacing OPC with calcined clays also improves compressive and flexural strength by generating additional C-S-H phases and densifying the microstructure. High-grade calcined clays further accelerate pozzolanic reactions, reducing pore connectivity and shrinkage and enhancing durability. Combining high-grade (95% metakaolin) with low-grade (50% metakaolin) calcined clays optimizes hardened characteristics, balancing strength and deformability. Integrating calcined clays into ternary systems with limestone powder enhances mechanical performance and reduces drying shrinkage, highlighting the need for a balance between rheological and mechanical characteristics [147].

Additionally, incorporating less than 1% nano clay (NC) has been found to enhance early-age mechanical properties and thixotropy at the micro level. The attraction between oppositely charged NC edges creates a denser microstructure, increasing static yield stress [148]. Research on GGBS-based cementitious mixes reveals its potential to improve early-age compressive strength and ultimate strength in geopolymers due to its latent hydraulic and pozzolanic properties, forming a homogeneous microstructure 3DPC. However, the concentration of GGBS should be carefully monitored to maintain final strength [149]. Furthermore, adding silica fume (SF) with smaller particle sizes enhances particle packing and is recommended at 10% for meeting extrudability [24]. Substituting 2% of OPC with silica fume can increase buildability by 117%, improving green strength and thixotropic properties [150]. Replacing 0-5% of fly ash with silica fume in the nano clay-modified mixture enhances yield stress, improving the shape stability of extruded layers and increasing the building rate [24].

10.1.2 Recycled aggregate

Researchers have utilized recycled aggregate and underused solids effectively in 3DCP [151]. For example, mine tailings improve mechanical and buildability qualities when 30% of sand is replaced [78]. Recycled rubber tyre powder has been used instead of fine sand, which, while reducing strength, enhances thermal insulation, acoustic, and ductility properties [152]. Lightweight mixtures have been developed using discarded glass and enlarged thermoplastic microspheres [153]. Additionally, recycled sand from leftover concrete has shown increased stiffness, while recycled glass has improved the buildability of the 3DPC mix [41, 154]. However, 3D-printed concrete with recycled sand exhibits lower compressive strength and variable flexural and splitting tensile strength results, although 3DPC with recycled sand shows improved microstructure [41, 154]. Despite natural aggregates being costlier, the use of recycled aggregates is increasing. More advancements are needed to achieve significant cost savings for complex structures in 3D-printed concrete compared to traditional methods [7]. Further investigation into recycled aggregate-based 3DPC is necessary. The basic properties of the sand used for 3DCP are presented in Table 8. Fig. 33 (a), (b), and (c) present test results for compressive, splitting tensile, and flexural strength of 3D printed concrete with varying recycled sand percentages [41].

Table 8 Basic properties of sand used for 3D concrete printing [41]

Type of sands	Fineness modulus	Maximum particle size (mm)	Apparent density (kg/m^3)	Loosely/dens packing density (kg/m^3)	Moisture content (%)	Water absorption (%)
Natural sand	1.62	0.9	2586.5	1399/1491	0.2	4.5
Recycled sand	1.53	0.9	2410.7	1014/1070	0.6	13.5

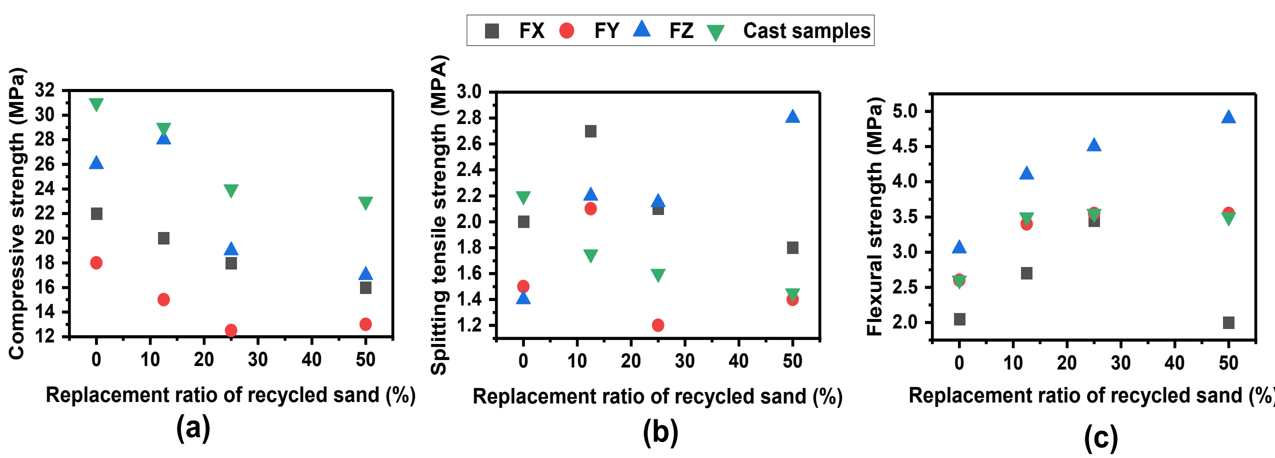

Fig. 33 Effect of different replacement ratios of recycled sand on (a) Compressive, (b) Splitting tensile, (c) Flexural strength [41]

As demonstrated in Fig. 33, the casted specimen achieved the highest compressive strength of 31.0 MPa at a 0% replacement ratio, while the Y-direction specimen had the lowest at 17.8 MPa. At a 50% replacement ratio, compressive strength dropped to 23.3 MPa for casted specimens and 13.3 MPa for printed specimens. Interestingly, at a 12.5% replacement ratio, compressive strength in the Z direction exceeded others. However, at 50% replacement, tensile splitting strength was significantly reduced by 37.6%. Flexural strength ranged from 2.1 MPa in the X direction to 3.2 MPa in the Z direction at 0% replacement, with maximum flexural strength reaching 4.5 MPa in the Z direction and 3.5 MPa in the X direction at 25% replacement, reflecting increases of 41.7% and 64.8% respectively.

10.1.3 Chemical admixtures

The inclusion of appropriate chemical admixtures is crucial in 3D concrete printing, significantly improving rheological and mechanical properties for extrusion and layer deposition. Accelerators such as potassium carbonate (K_2CO_3), calcium nitrate ($Ca(NO_3)_2$), sodium carbonate (Na_2CO_3), and triethanolamine (TEA) can regulate setting times between 5 to 150 minutes depending on dosages [155]. Calcium sulfoaluminate acts as an effective accelerator, while tartaric acid serves as a retarder to enhance printability [156, 157]. Polycarboxylic-based superplasticisers are recommended for maintaining flowability at low water-binder ratios [63, 64], and hydroxypropyl methylcellulose thickens mixtures, while viscosity-modifying agents (VMAs) enhance plastic viscosity and structural integrity during printing [47, 105].

Additionally, novel materials like magnetorheological cementitious inks (MRCIs) enable active rheological regulation via external magnetic fields, combining ferromagnetic components for a transition from fluid to solid upon activation. These inks improve yield stress and viscosity, facilitating complex geometries in 3D and 4D printing [158]. Polysaccharides like xanthan gum (XG) also modify rheology, enhancing yield stress and viscosity through hydrogen bond formation with water, improving filament integrity and operational duration [159].

Innovations such as the Quick Mixing Method further enhance the effectiveness of rheological modifiers like carboxymethylcellulose (CMC) and nano clay by improving dispersion in shorter mixing periods. CMC increases viscosity through polymer entanglement, while nano clay strengthens buildability due to its unique structure [160]. Finally, sodium carboxymethyl starch boosts water retention in slag-based geopolymer concrete [93]. Overall, these advancements highlight the crucial role of chemical admixtures in enhancing the printability and efficiency of 3D concrete printing.

10.2 Lightweight printable concrete

Rahul and Santhanam (2020) found that substituting sand with lightweight expanded clay aggregate (LECA) in 3D-printed concrete improved extrudability and printability at a 30% replacement level; however, segregation was noticed with more lightweight material [63]. Similarly, Falliano et al. (2020) observed excellent dimensional stability without slump in 3D-printed lightweight foamed concrete (3DP-LWFC), which showed no deformation [161]. In another study, Sun et al. (2021) used PVA fiber for ductile reinforcement and strain hardening, which reduced density and setting time while improving mechanical behavior. The printed specimen could withstand greater UCS loads when the fiber orientation was parallel to the loading direction [145].

10.3 Reinforced 3D concrete printing

Researchers have used various methods of reinforcement in 3DCP, as shown in Fig. 34. In Fig. 34(a), cable, as reinforcement, is fed at the print head by an extruder driven by a step motor [162]. To fix the cable at the center of the layer, one concentric pipe is developed and placed in the nozzle at an inclination. As shown in Fig. 34(d), printing over conventional bar, bars are placed on the printed layer, then another layer of printing is done. Another method of reinforcement used is reinforcing after the printing of the concrete, as shown in Figs 34(b) and (e). In this method, a device is attached to the print head. This method uses reinforcement in the form of steel nails, steel fibers, or stapling to increase the flexural strength and ductility of the 3D-printed concrete [163, 164]. In another method of reinforcing, mesh reinforcement is embedded in the concrete layer through a customized nozzle shown in Fig. 34(c). Meshes were overlapped to provide continuous reinforcement. Fig. 34(f) depicts the pre-installed reinforcement, in which first reinforcement is installed manually, then two nozzles on either side of the reinforcement are installed to print the concrete layer by layer [165]. Researchers have used glass, basalt, carbon, poly-vinyl alcohol, and polyethylene fibers as reinforcement to enhance the mechanical properties of 3D-printed concrete [124, 155, 166]. As shown in Fig. 34(g), fibers were placed along the printing direction.

Based on the methods/type of reinforcement, properties are discussed in Table 9.

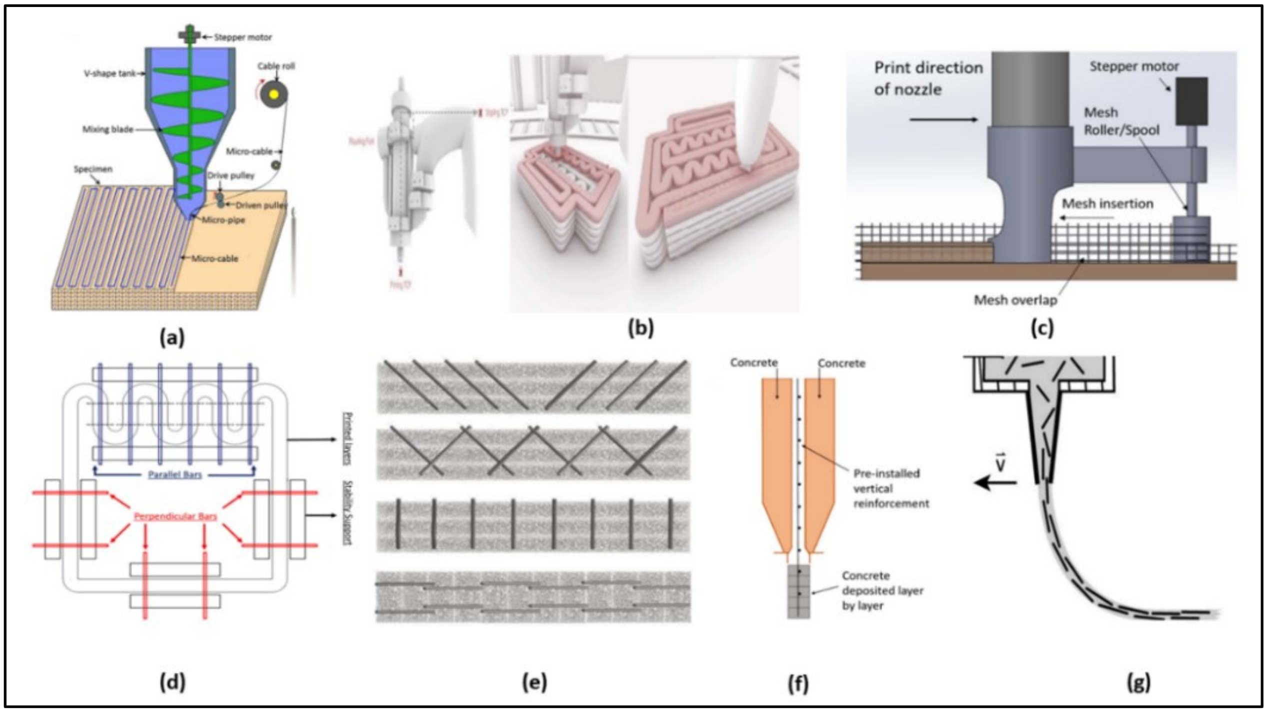

Fig. 34 Reinforcement methods (a) Insertion of cable at the nozzle [162], **(b) Reinforcement in staple form after printing** [164], **(c) Insertion of mesh during printing through custom-designed nozzle** [165], **(d) Printing over conventional bar** [167], **(e) Manual insertion of nails during printing** [163], **(f) pre-installed reinforcement** [165], **and (g) Fiber mixed with material** [168]

Table 9 Reinforcement method and their effects on the concrete properties

Sl. No.	Methods/Types of Reinforcement	Properties	References
1.	Insertion of cable at the nozzle	- Tensile and flexural strength Increased up to 290% - Bond strength decreased - Ductility and Porosity increased	[95, 169]
2.	Insertion of reinforcement after printing	- Increased flexural strength and ductility using steel nails, fibers, or stapling	[163, 164]
3.	Mesh reinforcement	- Increased flexural strength by up to 290% - Ductility increased	[9, 165]
4.	Printing over the conventional bar	- Bond strength and Ductility Increased	[194]
5.	Printed reinforcement	- Similar bond strength and ductility to conventional steel bar - Higher flexural strength	[9, 170]
6.	Fiber reinforcement	- Increased tensile and flexural strength with various fibers - Crack formation reduced	[124, 155, 166]

11 Conventional v/s 3D printed concrete

11.1 Life cycle costing

Labor, supplies, and equipment are the primary costs in traditional building [3]. In a conventional structure, labor and materials make up over half of the total cost, with equipment accounting for about 20%. For 3D printed concrete, material costs rise to around 50%, while labor decreases to 35%, and equipment costs drop by 20% [3]. The necessity of formwork in traditional construction drives these costs up. Unlike traditional methods, 3D printing eliminates the need for formwork, significantly reducing costs. While 3D printed concrete can be cheaper due to reduced waste and over-engineering, using expensive additives like nano-clay may increase costs [3, 38]. Researchers have analyzed the material and construction costs for 3DPC, as shown in Fig. 35. The findings by Soto et al. [171] and Weng et al. [100] indicate that 3DCP construction costs are high due to the use of robotic arm-type 3D concrete printers, unlike the gantry-type used by other researchers.

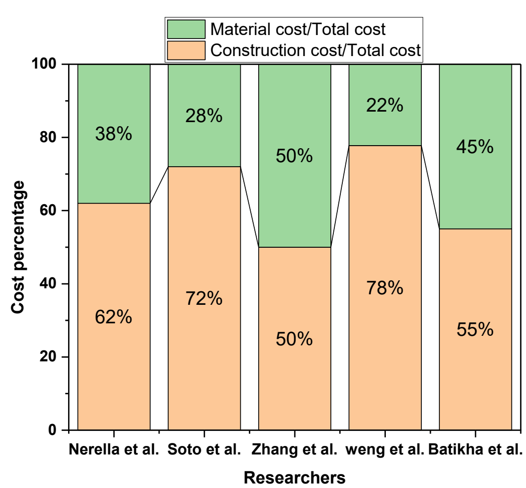

Fig. 35 Relative percentage of material cost and construction cost in 3DCP reported by different researchers [38, 100, 171–173]

11.2 Life cycle analysis

Cement content is a key variable in construction that affects the environment, with 3D printing having a greater detrimental effect than conventional methods due to its higher cement requirements [7, 54, 174, 175]. Alternatives like limestone calcined clay cement and supplementary cementitious materials (SCMs) such as fly ash, metakaolin, and silica fume can help reduce environmental impacts [7], such as global warming potential (GWP), Greenhouse gas emission (GHG), Acidification potential (AP), Eutrophication potential (EP), Ozone depletion (OD), Particulate matter (PM), Fossil fuel depletion (FFD), Smog formation potential (SFP), etc. of 3D printed concrete using OPC and supplementary cementitious material, and their comparison with respect to conventional concrete is given in Table 10.

Table 10 Comparison of the environmental impact of conventional and 3D-printed concrete

Researchers	Materials used/method	3DCP environmental impact as compared to conventional concrete							
		GWP	GHG	AP	EP	SFP	FFD	OD	PM
Han et al. [7] Yao et al. [174] Alhumayani et al. [175]	Ordinary Portland cement	↑	↑					↑	
Alhumayani et al. [175]	Cob	↓						↓	↓
Long et al. [54]	LC^3		↓						
Yao et al. [174]	Geopolymer concrete,		↑						
Mohammad et al. [176]	Sand replaced with expanded perlite (EXP)	↓		↓	↓	↓	↓		
Han et al. [7]	Recycled aggregate	↓	↓						
Juan et al. [4]	By reducing thickness		↓						
Alhumayani et al. [175] and Nerella et al. [172]	Replacement of cement by fly ash and silica fume				↓			↓	↓
Weng et al. [177]	Elimination of formwork		↓						
Markin et al. [178]	Foam concrete		↑						
Long et al. [162]	Microcrystalline cellulose (MCC)		↓						

Using LC_3 can cut GHG and energy consumption by 50.2% and 45.2%, respectively [54]. Additionally, Cob as an SCM has been shown to reduce GWP, ozone depletion, and particulate matter [175]. Yao et al. [174] indicated that while geopolymer concrete has a high initial environmental impact, this can be mitigated with an alkaline activator. The use of larger aggregates is restricted in 3D printed concrete, resulting in greater strength compared to conventional concrete [174]. Reducing layer thickness can also lower CO_2 emissions [4]. Mohammad et al. [176] found that using expanded perlite instead of sand reduced air pollution, eutrophication potential (EP), and smog formation potential (SFP) emissions by 50–55%. Furthermore, 3D printed concrete can lower EP emissions by 28% and slightly reduce AP and SFP rates compared to traditional concrete. According to Markets and Markets [38], 3D printing can save construction time by 50 to 70%, labor costs by 50 to 80%, and waste output by up to 60%. Conventional concrete involves formwork, which accounts for 40% of total construction costs and contributes to global warming and GHG emissions [179]. Eliminating formwork reduces CO_2 production by 89.2% [177], while microcrystalline cellulose (MCC) use can reduce CO_2 by 6.82% [180]. Although foam concrete increases CO_2 emissions, it also enhances thermal performance [173]. Kantumuchu [181] projected that 3D printing could save $170 to $593 billion, reduce the world's main energy supply by 2.54 to 9.30 EJ, and decrease CO_2 emissions by 130.5 to 525.5 Mt by 2025. In Fig. 36, the life cycle of a 3D-printed structure is depicted schematically.

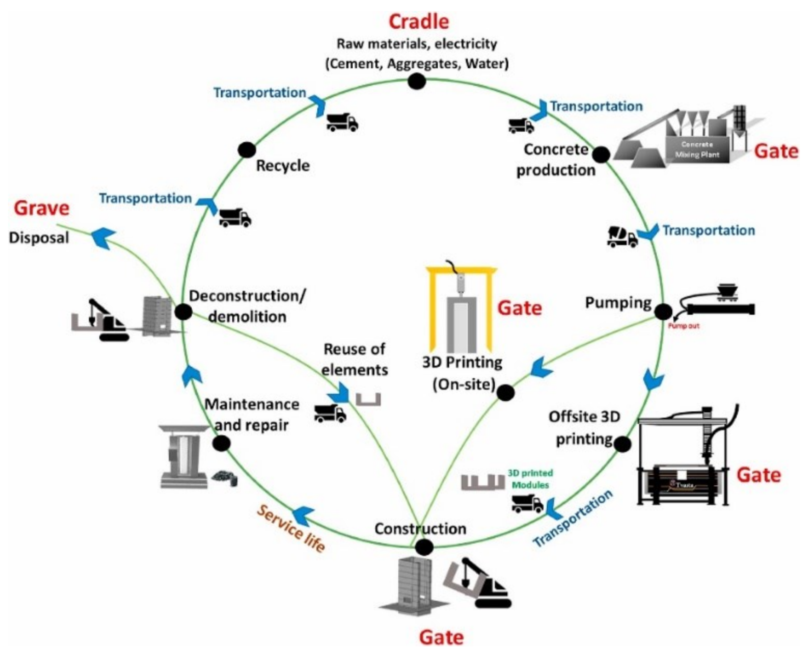

Fig. 36 Life cycle of a 3D printed structure [46]

Sustainability evaluation begins with defining system boundaries, which can be classified into cradle-to-grave, cradle-to-gate, gate-to-gate, and cradle-to-cradle. The cradle-to-gate approach is essential as it encompasses the phases from mining to either manufacturing or onsite construction, while gate-to-gate provides precise analysis without much guesswork regarding raw materials and extraction methods. The cradle-to-grave approach is less useful due to challenges in predicting end-of-life processes, making cradle-to-cradle, though uncommon in the building sector, an ideal method to initiate a new cycle post-completion [46].

3DCP reduces building time by about 95% compared to cast-in-situ reinforced concrete (RC), cold-formed steel (CFS), and hot-rolled steel (HRS), with the exception of PMC [173]. Furthermore, 3DCP offers significant cost savings and is comparable to CFS while achieving a 32% reduction in CO_2 emissions. In terms of weight, steel structures are 34% lighter than 3DCP, while precast modular concrete is 35% heavier, making it the heaviest method. Cast-in-situ RC structures have a weight similar to that of 3DCP.

12 Prospects for future study

3DCP is an innovative construction technique that could significantly impact the construction industry and help achieve sustainability goals, including net-zero emissions by 2050. Its promise hinges on automated prefabrication technologies that facilitate the transition from factory manufacturing to on-site construction. However, advancements in equipment, control systems, and printing resolution are essential to unlock its full potential across various practical applications. Currently, the lack of specifications, design standards, and underdeveloped regulations poses challenges to the commercialization and adoption of large-scale 3D printing technologies. Addressing these issues is crucial for maximizing the benefits of 3DCP in mainstream construction. Sustainability efforts in 3D printing include minimizing binder usage, exploring renewable binding materials, and sourcing local materials, all of which align with broader sustainability objectives. One notable area for improvement is reinforcement methods for 3DCP structures, where research should focus on automating operations to ensure structural integrity while maintaining economy and sustainability. Although progress has been made in assessing the environmental impact of 3DCP, a deeper investigation into its life cycle evaluation is necessary to provide insights into its overall sustainability and inform future developments. Looking ahead, expanding 3DCP applications to include the renovation of existing buildings would offer significant potential for restoring old structures.

13 Conclusions and recommendations

From the review of the research that has been done on the swiftly developing 3DCP technology, the following conclusions and recommendations can be made.

- Rheological and mechanical properties have contradictory results due to the various printing parameters and mix design strategies used by researchers. The mixing and printing procedure should be standardized.
- 3DCP requires significant cementitious material, leading to higher costs and carbon emissions. Supplementary materials like fly ash, GGBS, and silica fumes are suggested as alternatives, though some are limited in availability. For long-term sustainability, researchers recommend exploring options like limestone-calcined clay cement.
- 3D concrete printing can be scaled up from paste/mortar to concrete by employing the concept of particle packing theory.
- The only method available for testing the mechanical properties is cutting the printed specimen into a cubical or cylindrical shape. This action may disturb the interlayer bonding of the printed specimen. An improved testing methodology must be developed.

- Due to the lack of proper reinforcement methods, the strength of structural element of 3D-printed concrete is less than that of conventional concrete. High-strength 3D-printed concrete is the need of the hour. Automated reinforcement methods in different forms are one of the major focuses of research.
- For longer gap time, extensive voids and the formation of calcite are seen as distinct interfaces on the layer in SEM image, which reduces the bond strength between layers. Apart from gap time, dehydration of the specimen has a great impact on flexural strength. It is seen from the optical microscopy image that the exposed sample has a smoother crack surface and a great void content as compared to the covered samples.
- Over half of conventional building costs come from labor and materials, with equipment accounting for about 20%. Formwork alone can make up 30-40% of structure costs. 3DCP eliminates formwork and reduces labor needs. In 3D printed concrete, material costs rise to around 50%, while labor decreases to 35% and equipment costs drop by 20%. By 2025, 3D printing could reduce costs by \$170 to \$593 billion and lower CO_2 emissions by 130.5 to 525.5 million tons.
- Freeze-thaw attack decreased the strength of 3DP concrete. By adding air-entraining admixtures, the strength of the concrete can be enhanced. At the interlayers, interconnected voids increase chloride ion infiltration. With longer interlayer gaps, chloride depth continues to rise, which makes concrete less durable.

Reference

1. Suntharalingam T, Nagaratnam B, Poologanathan K, et al (2019) Evolution of additive manufacturing technology in construction industry & challenges on implementation: A review. 10th Int Conf Struct Eng Constr Manag
2. Allouzi R, Azhari W Al, Allouzi R (2020) Conventional Construction and 3D Printing: A Comparison Study on Material Cost in Jordan. J Eng (United Kingdom) 2020:. https://doi.org/10.1155/2020/1424682
3. Tay YWD, Panda B, Paul SC, et al (2017) 3D printing trends in building and construction industry: a review. Virtual Phys Prototyp 12:261–276. https://doi.org/10.1080/17452759.2017.1326724
4. Agustí-Juan I, Müller F, Hack N, et al (2017) Potential benefits of digital fabrication for complex structures: Environmental assessment of a robotically fabricated concrete wall. J Clean Prod 154:330–340. https://doi.org/10.1016/J.JCLEPRO.2017.04.002
5. Lowke D, Talke D, Dressler I, et al (2020) Particle bed 3D printing by selective cement activation – Applications, material and process technology. Cem Concr Res 134:106077. https://doi.org/10.1016/J.CEMCONRES.2020.106077
6. Lu Y, Xiao J, Li Y (2024) 3D printing recycled concrete incorporating plant fibres: A comprehensive review. Constr Build Mater 425:135951. https://doi.org/10.1016/j.conbuildmat.2024.135951
7. Han Y, Yang Z, Ding T, Xiao J (2021) Environmental and economic assessment on 3D printed buildings with recycled concrete. J Clean Prod 278:123884. https://doi.org/10.1016/J.JCLEPRO.2020.123884
8. Soltan DG, Li VC (2018) A self-reinforced cementitious composite for building-scale 3D printing. Cem Concr Compos 90:1–13. https://doi.org/10.1016/J.CEMCONCOMP.2018.03.017
9. Mechtcherine V, Grafe J, Nerella VN, et al (2018) 3D-printed steel reinforcement for digital concrete construction – Manufacture, mechanical properties and bond behaviour. Constr Build Mater 179:125–137. https://doi.org/10.1016/J.CONBUILDMAT.2018.05.202
10. Baz B, Remond S, Aouad G (2022) Influence of the mix composition on the thixotropy of 3D printable mortars. Mag Concr Res 74:271–283. https://doi.org/10.1680/jmacr.20.00193
11. Xiao J, Ji G, Zhang Y, et al (2021) Large-scale 3D printing concrete technology: Current status and future opportunities. Cem Concr Compos 122:104115. https://doi.org/10.1016/j.cemconcomp.2021.104115
12. Dizon JRC, Gache CCL, Cascolan HMS, et al (2021) Post-Processing of 3D-Printed Polymers. Technologies 9:61. https://doi.org/10.3390/technologies9030061
13. Nerella VN, Mechtcherine V (2019) Studying the Printability of Fresh Concrete for Formwork-Free

Concrete Onsite 3D Printing Technology (CONPrint3D). 3D Concr Print Technol 333–347. https://doi.org/10.1016/B978-0-12-815481-6.00016-6

14. Huang S, Xu W, Li Y (2022) The impacts of fabrication systems on 3D concrete printing building forms. Front Archit Res 11:653–669. https://doi.org/10.1016/J.FOAR.2022.03.004
15. Khoshnevis B (2004) Automated construction by contour crafting—related robotics and information technologies. Autom Constr 13:5–19. https://doi.org/10.1016/J.AUTCON.2003.08.012
16. Al Jassmi H, Al Najjar F, Mourad AHI (2018) Large-Scale 3D Printing: The Way Forward. IOP Conf Ser Mater Sci Eng 324:. https://doi.org/10.1088/1757-899X/324/1/012088
17. Souza MT, Ferreira IM, Guzi de Moraes E, et al (2020) 3D printed concrete for large-scale buildings: An overview of rheology, printing parameters, chemical admixtures, reinforcements, and economic and environmental prospects. J Build Eng 32:101833. https://doi.org/10.1016/J.JOBE.2020.101833
18. Zhang X, Li M, Lim JH, et al (2018) Large-scale 3D printing by a team of mobile robots. Autom Constr 95:98–106. https://doi.org/10.1016/J.AUTCON.2018.08.004
19. Paul SC, van Zijl GPAG, Gibson I (2018) A review of 3D concrete printing systems and materials properties: current status and future research prospects. Rapid Prototyp J 24:784–798. https://doi.org/10.1108/RPJ-09-2016-0154
20. Zhang N, Sanjayan J (2023) Extrusion nozzle design and print parameter selections for 3D concrete printing. Cem Concr Compos 137:104939. https://doi.org/10.1016/j.cemconcomp.2023.104939
21. Xiao J, Zou S, Yu Y, et al (2020) 3D recycled mortar printing: System development, process design, material properties and on-site printing. J Build Eng 32:101779. https://doi.org/10.1016/J.JOBE.2020.101779
22. Jo JH, Jo BW, Cho W, Kim JH (2020) Development of a 3D Printer for Concrete Structures: Laboratory Testing of Cementitious Materials. Int J Concr Struct Mater 14:. https://doi.org/10.1186/s40069-019-0388-2
23. Panda B, Mohamed NAN, Paul SC, et al (2019) The effect of material fresh properties and process parameters on buildability and interlayer adhesion of 3D printed concrete. Materials (Basel) 12:. https://doi.org/10.3390/ma12132149
24. Wolfs RJM, Bos FP, Salet TAM (2018) Early age mechanical behaviour of 3D printed concrete: Numerical modelling and experimental testing. Cem Concr Res 106:103–116. https://doi.org/10.1016/J.CEMCONRES.2018.02.001
25. Panda B, Paul SC, Mohamed NAN, et al (2018) Measurement of tensile bond strength of 3D printed geopolymer mortar. Measurement 113:108–116. https://doi.org/10.1016/J.MEASUREMENT.2017.08.051
26. Paul SC, Tay YWD, Panda B, Tan MJ (2018) Fresh and hardened properties of 3D printable cementitious materials for building and construction. Arch Civ Mech Eng 18:311–319. https://doi.org/10.1016/j.acme.2017.02.008
27. Lyu Fuyan, Zhao Dongliang , Hou Xiaohui SL and ZQ (2021) applied sciences Overview of the Development of 3D-Printing Concrete : Applie Sci
28. Zielinski A, Kaszynska M, Skibicki S, Olczyk N (2019) Development of Autogenous Shrinkage Deformation and Strength Parameters in Self-Consolidating Concrete with Light and Natural Aggregate. IOP Conf Ser Mater Sci Eng 471:. https://doi.org/10.1088/1757-899X/471/3/032019
29. Tay YWD, Li MY, Tan MJ (2019) Effect of printing parameters in 3D concrete printing: Printing region and support structures. J Mater Process Technol 271:261–270. https://doi.org/10.1016/J.JMATPROTEC.2019.04.007
30. Manikandan K, Jiang X, Singh AA, et al (2020) Effects of Nozzle Geometries on 3D Printing of Clay Constructs: Quantifying Contour Deviation and Mechanical Properties. Procedia Manuf 48:678–683. https://doi.org/10.1016/J.PROMFG.2020.05.160
31. Lu B, Li M, Wong TN, Qian S (2021) Effect of printing parameters on material distribution in spray-based 3D concrete printing (S-3DCP). Autom Constr 124:103570. https://doi.org/10.1016/J.AUTCON.2021.103570
32. Bai G, Wang L, Wang F, Ma G (2021) In-process reinforcing method: dual 3D printing procedure for ultra-high performance concrete reinforced cementitious composites. Mater Lett 304:130594. https://doi.org/10.1016/j.matlet.2021.130594
33. Ji G, Ding T, Xiao J, et al (2019) A 3D Printed Ready-Mixed Concrete Power Distribution Substation: Materials and Construction Technology. Materials (Basel) 12:1540. https://doi.org/10.3390/ma12091540
34. Tao Y, Lesage K, Van Tittelboom K, et al (2023) Twin-pipe pumping strategy for stiffening control of 3D printable concrete: From transportation to fabrication. Cem Concr Res 168:107137. https://doi.org/10.1016/j.cemconres.2023.107137

35. Wangler T, Pileggi R, Gürel S, Flatt RJ (2022) A chemical process engineering look at digital concrete processes: critical step design, inline mixing, and scaleup. Cem Concr Res 155:106782. https://doi.org/10.1016/j.cemconres.2022.106782
36. Zhang N, Sanjayan J (2024) Pumping-less 3D concrete printing using quick nozzle mixing. Autom Constr 166:105609. https://doi.org/10.1016/j.autcon.2024.105609
37. Zhang N, Xia M, Sanjayan J (2022) Short-duration near-nozzle mixing for 3D concrete printing. Cem Concr Res 151:106616. https://doi.org/10.1016/j.cemconres.2021.106616
38. Zhang J, Wang J, Dong S, et al (2019) A review of the current progress and application of 3D printed concrete. Compos Part A Appl Sci Manuf 125:105533. https://doi.org/10.1016/J.COMPOSITESA.2019.105533
39. Bong SH, Xia M, Nematollahi B, Shi C (2021) Ambient temperature cured 'just-add-water' geopolymer for 3D concrete printing applications. Cem Concr Compos 121:104060. https://doi.org/10.1016/J.CEMCONCOMP.2021.104060
40. Hojati M, Li Z, Memari AM, et al (2022) 3D-printable quaternary cementitious materials towards sustainable development: Mixture design and mechanical properties. Results Eng 13:100341. https://doi.org/10.1016/J.RINENG.2022.100341
41. Ding T, Xiao J, Zou S, Wang Y (2020) Hardened properties of layered 3D printed concrete with recycled sand. Cem Concr Compos 113:103724. https://doi.org/10.1016/J.CEMCONCOMP.2020.103724
42. Marchment T, Sanjayan J, Xia M (2019) Method of enhancing interlayer bond strength in construction scale 3D printing with mortar by effective bond area amplification. Mater Des 169:107684. https://doi.org/10.1016/J.MATDES.2019.107684
43. Nerella VN, Näther M, Iqbal A, et al (2019) Inline quantification of extrudability of cementitious materials for digital construction. Cem Concr Compos 95:260–270. https://doi.org/10.1016/J.CEMCONCOMP.2018.09.015
44. Zhao Z, Chen M, Xu J, et al (2021) Mix design and rheological properties of magnesium potassium phosphate cement composites based on the 3D printing extrusion system. Constr Build Mater 284:122797. https://doi.org/10.1016/J.CONBUILDMAT.2021.122797
45. Wang X, Jia L, Jia Z, et al (2022) Optimization of 3D printing concrete with coarse aggregate via proper mix design and printing process. J Build Eng 56:104745. https://doi.org/10.1016/J.JOBE.2022.104745
46. Bhattacherjee S, Basavaraj AS, Rahul A V., et al (2021) Sustainable materials for 3D concrete printing. Cem Concr Compos 122:104156. https://doi.org/10.1016/J.CEMCONCOMP.2021.104156
47. Chen Y, Figueiredo SC, Yalçinkaya Ç, et al (2019) The effect of viscosity-modifying admixture on the extrudability of limestone and calcined clay-based cementitious material for extrusion-based 3D concrete printing. Materials (Basel) 12:9–12. https://doi.org/10.3390/ma12091374
48. Xiao J (2018) Erratum to: Recycled Aggregate Concrete Structures. pp E1–E1
49. Zou S, Xiao J, Ding T, et al (2021) Printability and advantages of 3D printing mortar with 100% recycled sand. Constr Build Mater 273:121699. https://doi.org/10.1016/j.conbuildmat.2020.121699
50. Fennis SAAM, Walraven JC (2012) Using particle packing technology for sustainable concrete mixture design. Heron 57:73–101
51. Campos HF, Klein NS, Marques Filho J, Bianchini M (2020) Low-cement high-strength concrete with partial replacement of Portland cement with stone powder and silica fume designed by particle packing optimization. J Clean Prod 261:121228. https://doi.org/10.1016/J.JCLEPRO.2020.121228
52. Mehdipour I, Khayat KH (2019) Elucidating how particle packing controls rheology and strength development of dense cementitious suspensions. Cem Concr Compos 104:103413. https://doi.org/10.1016/J.CEMCONCOMP.2019.103413
53. Chung SY, Kim JS, Lehmann C, et al (2020) Investigation of phase composition and microstructure of foamed cement paste with different supplementary cementing materials. Cem Concr Compos 109:103560. https://doi.org/10.1016/J.CEMCONCOMP.2020.103560
54. Long WJ, Lin C, Tao JL, et al (2021) Printability and particle packing of 3D-printable limestone calcined clay cement composites. Constr Build Mater 282:122647. https://doi.org/10.1016/J.CONBUILDMAT.2021.122647
55. Mai I, Brohmann L, Freund N, et al (2021) Viable Solution. 1–22
56. Chen Y, Zhang Y, Pang B, et al (2021) Extrusion-based 3D printing concrete with coarse aggregate: Printability and direction-dependent mechanical performance. Constr Build Mater 296:123624. https://doi.org/10.1016/J.CONBUILDMAT.2021.123624
57. Arunothayan AR, Nematollahi B, Ranade R, et al (2020) Development of 3D-printable ultra-high

performance fiber-reinforced concrete for digital construction. Constr Build Mater 257:119546. https://doi.org/10.1016/J.CONBUILDMAT.2020.119546

58. Van Der Putten J, De Schutter G, Van Tittelboom K (2019) Surface modification as a technique to improve inter-layer bonding strength in 3d printed cementitious materials. RILEM Tech Lett 4:33–38. https://doi.org/10.21809/rilemtechlett.2019.84
59. Ramakrishnan S, Kanagasuntharam S, Sanjayan J (2022) In-line activation of cementitious materials for 3D concrete printing. Cem Concr Compos 131:104598. https://doi.org/10.1016/J.CEMCONCOMP.2022.104598
60. Perrot A, Rangeard D, Pierre A (2016) Structural built-up of cement-based materials used for 3D-printing extrusion techniques. Mater Struct Constr 49:1213–1220. https://doi.org/10.1617/s11527-015-0571-0
61. Vasileios S, Charrier M, Ouellet-Plamondon CM (2020) Prediction of the Yield Stress of Printing Mortar Ink. Springer International Publishing
62. Andrew Ting GH, Noel Quah TK, Lim JH, et al (2022) Extrudable region parametrical study of 3D printable concrete using recycled glass concrete. J Build Eng 50:104091. https://doi.org/10.1016/J.JOBE.2022.104091
63. Rahul A V., Santhanam M (2020) Evaluating the printability of concretes containing lightweight coarse aggregates. Cem Concr Compos 109:103570. https://doi.org/10.1016/J.CEMCONCOMP.2020.103570
64. Li Z, Ma G, Wang F, et al (2022) Expansive cementitious materials to improve micro-cable reinforcement bond in 3D concrete printing. Cem Concr Compos 125:104304. https://doi.org/10.1016/J.CEMCONCOMP.2021.104304
65. Muthukrishnan S, Ramakrishnan S, Sanjayan J (2022) Set on demand geopolymer using print head mixing for 3D concrete printing. Cem Concr Compos 128:104451. https://doi.org/10.1016/J.CEMCONCOMP.2022.104451
66. Zhu B, Pan J, Zhou Z, Cai J (2021) Mechanical properties of engineered cementitious composites beams fabricated by extrusion-based 3D printing. Eng Struct 238:112201. https://doi.org/10.1016/J.ENGSTRUCT.2021.112201
67. Bao Y, Xu M, Soltan D, et al (2019) Three-dimensional printing multifunctional engineered cementitious composites (ECC) for structural elements. Springer International Publishing
68. Panda B, Tan MJ (2018) Experimental study on mix proportion and fresh properties of fly ash based geopolymer for 3D concrete printing. Ceram Int 44:10258–10265. https://doi.org/10.1016/J.CERAMINT.2018.03.031
69. Le TT, Austin SA, Lim S, et al (2012) Mix design and fresh properties for high-performance printing concrete. Mater Struct Constr 45:1221–1232. https://doi.org/10.1617/s11527-012-9828-z
70. Vikan H, Jacobsen S (2010) Influence of rheology on the pumpability of mortar
71. Mohan MK, Rahul A V., Van Tittelboom K, De Schutter G (2020) Evaluating the Influence of Aggregate Content on Pumpability of 3D Printable Concrete. Springer International Publishing
72. Chaves Figueiredo S, Romero Rodríguez C, Ahmed ZY, et al (2019) An approach to develop printable strain hardening cementitious composites. Mater Des 169:107651. https://doi.org/10.1016/J.MATDES.2019.107651
73. Mechtcherine V, Nerella VN, Kasten K (2014) Testing pumpability of concrete using Sliding Pipe Rheometer. Constr Build Mater 53:312–323. https://doi.org/10.1016/J.CONBUILDMAT.2013.11.037
74. Nerella VN, Mechtcherine V (2018) Virtual Sliding Pipe Rheometer for estimating pumpability of concrete. Constr Build Mater 170:366–377. https://doi.org/10.1016/J.CONBUILDMAT.2018.03.003
75. Tay YWD, Qian Y, Tan MJ (2019) Printability region for 3D concrete printing using slump and slump flow test. Compos Part B Eng 174:106968. https://doi.org/10.1016/J.COMPOSITESB.2019.106968
76. Chhabra RP, Richardson JF (2011) Non-Newtonian flow and applied rheology: engineering applications. Butterworth-Heinemann
77. Rehman AU, Kim J-H (2021) 3D Concrete Printing: A Systematic Review of Rheology
78. Álvarez-Fernández MI, Prendes-Gero MB, González-Nicieza C, et al (2021) Optimum mix design for 3D concrete printing using mining tailings: A case study in Spain. Sustain 13:1–14. https://doi.org/10.3390/su13031568
79. Gołaszewski J, Szwabowski J (2004) Influence of superplasticizers on rheological behaviour of fresh cement mortars. Cem Concr Res 34:235–248. https://doi.org/10.1016/j.cemconres.2003.07.002
80. Lipscomb GG, Denn MM (1984) Flow of bingham fluids in complex geometries. J Nonnewton Fluid Mech 14:337–346. https://doi.org/10.1016/0377-0257(84)80052-X
81. Jayathilakage R, Rajeev P, Sanjayan J (2020) Yield stress criteria to assess the buildability of 3D concrete printing. Constr Build Mater 240:117989. https://doi.org/10.1016/J.CONBUILDMAT.2019.117989

82. Ooms T, Vantyghem G, Van Coile R, De Corte W (2021) A parametric modelling strategy for the numerical simulation of 3D concrete printing with complex geometries. Addit Manuf 38:101743. https://doi.org/10.1016/j.addma.2020.101743
83. Vantyghem G, Ooms T, De Corte W (2021) VoxelPrint: A Grasshopper plug-in for voxel-based numerical simulation of concrete printing. Autom Constr 122:103469. https://doi.org/10.1016/j.autcon.2020.103469
84. Liu H, Ding T, Xiao J, Mechtcherine V (2022) Buildability prediction of 3D–printed concrete at early-ages: A numerical study with Drucker–Prager model. Addit Manuf 55:102821. https://doi.org/10.1016/j.addma.2022.102821
85. De Schutter G, Lesage K, Mechtcherine V, et al (2018) Vision of 3D printing with concrete — Technical, economic and environmental potentials. Cem Concr Res 112:25–36. https://doi.org/10.1016/J.CEMCONRES.2018.06.001
86. Moeini MA, Hosseinpoor M, Yahia A (2020) Effectiveness of the rheometric methods to evaluate the build-up of cementitious mortars used for 3D printing. Constr Build Mater 257:119551. https://doi.org/10.1016/J.CONBUILDMAT.2020.119551
87. Zhang Y, Zhang Y, She W, et al (2019) Rheological and harden properties of the high-thixotropy 3D printing concrete. Constr Build Mater 201:278–285. https://doi.org/10.1016/J.CONBUILDMAT.2018.12.061
88. Widyatmoko I, Hoang N-D, Pham A-D, et al (2003) Summary of concrete workability test methods. Constr Build Mater 34:118180
89. Rahul A V., Santhanam M, Meena H, Ghani Z (2019) 3D printable concrete: Mixture design and test methods. Cem Concr Compos 97:13–23. https://doi.org/10.1016/J.CEMCONCOMP.2018.12.014
90. Kruger J, Zeranka S, van Zijl G (2019) An ab initio approach for thixotropy characterisation of (nanoparticle-infused) 3D printable concrete. Constr Build Mater 224:372–386. https://doi.org/10.1016/J.CONBUILDMAT.2019.07.078
91. Kruger J, Cho S, Zeranka S, et al (2020) 3D concrete printer parameter optimisation for high rate digital construction avoiding plastic collapse. Compos Part B Eng 183:107660. https://doi.org/10.1016/J.COMPOSITESB.2019.107660
92. Papachristoforou M, Mitsopoulos V, Stefanidou M (2018) Evaluation of workability parameters in 3D printing concrete. Procedia Struct Integr 10:155–162. https://doi.org/10.1016/J.PROSTR.2018.09.023
93. Sun C, Xiang J, Xu M, et al (2020) 3D extrusion free forming of geopolymer composites: Materials modification and processing optimization. J Clean Prod 258:120986. https://doi.org/10.1016/J.JCLEPRO.2020.120986
94. Nair SAO, Panda S, Santhanam M, et al (2020) A critical examination of the influence of material characteristics and extruder geometry on 3D printing of cementitious binders. Cem Concr Compos 112:103671. https://doi.org/10.1016/J.CEMCONCOMP.2020.103671
95. Chen M, Yang L, Zheng Y, et al (2020) Yield stress and thixotropy control of 3D-printed calcium sulfoaluminate cement composites with metakaolin related to structural build-up. Constr Build Mater 252:119090. https://doi.org/10.1016/J.CONBUILDMAT.2020.119090
96. Chen M, Li L, Wang J, et al (2020) Rheological parameters and building time of 3D printing sulphoaluminate cement paste modified by retarder and diatomite. Constr Build Mater 234:117391. https://doi.org/10.1016/J.CONBUILDMAT.2019.117391
97. Chen M, Liu B, Li L, et al (2020) Rheological parameters, thixotropy and creep of 3D-printed calcium sulfoaluminate cement composites modified by bentonite. Compos Part B Eng 186:107821. https://doi.org/10.1016/J.COMPOSITESB.2020.107821
98. Le TT, Austin SA, Lim S, et al (2012) Hardened properties of high-performance printing concrete. Cem Concr Res 42:558–566. https://doi.org/10.1016/J.CEMCONRES.2011.12.003
99. Jayathilakage R, Sanjayan J, Rajeev P (2018) Comparison of rheology measurement techniques used in extrusion based concrete 3D printing. Springer Singapore
100. Weng Y, Li M, Tan MJ, Qian S (2018) Design 3D printing cementitious materials via Fuller Thompson theory and Marson-Percy model. Constr Build Mater 163:600–610. https://doi.org/10.1016/J.CONBUILDMAT.2017.12.112
101. Lafhaj Z, Rabenantoandro AZ, el Moussaoui S, et al (2019) Experimental approach for printability assessment: Toward a practical decision-making framework of printability for cementitious materials. Buildings 9:. https://doi.org/10.3390/buildings9120245
102. Chougan M, Hamidreza Ghaffar S, Jahanzat M, et al (2020) The influence of nano-additives in strengthening mechanical performance of 3D printed multi-binder geopolymer composites. Constr Build

Mater 250:118928. https://doi.org/10.1016/J.CONBUILDMAT.2020.118928
103. Lee H, Kim JHJ, Moon JH, et al (2019) Evaluation of the mechanical properties of a 3D-printed mortar. Materials (Basel) 12:1–13. https://doi.org/10.3390/ma1224104
104. Cho S, Kruger J, van Rooyen A, et al (2020) Rheology of 3D Printable Lightweight Foam Concrete Incorporating Nano-Silica. Springer International Publishing
105. Chen Y, Chaves Figueiredo S, Li Z, et al (2020) Improving printability of limestone-calcined clay-based cementitious materials by using viscosity-modifying admixture. Cem Concr Res 132:106040. https://doi.org/10.1016/J.CEMCONRES.2020.106040
106. Kaszyńska M, Hoffmann M, Skibicki S, et al (2018) Evaluation of suitability for 3D printing of high performance concretes. MATEC Web Conf 163:1–8. https://doi.org/10.1051/matecconf/201816301002
107. Chen Y, He S, Zhang Y, et al (2021) 3D printing of calcined clay-limestone-based cementitious materials. Cem Concr Res 149:106553. https://doi.org/10.1016/J.CEMCONRES.2021.106553
108. Pan T, Jiang Y, He H, et al (2021) Effect of structural build-up on interlayer bond strength of 3d printed cement mortars. Materials (Basel) 14:1–17. https://doi.org/10.3390/ma14020236
109. Newman J, Choo BS (2003) Advanced concrete technology 3: processes. Elsevier
110. Buswell RA, Leal de Silva WR, Jones SZ, Dirrenberger J (2018) 3D printing using concrete extrusion: A roadmap for research. Cem Concr Res 112:37–49. https://doi.org/10.1016/J.CEMCONRES.2018.05.006
111. Van Der Putten J, Deprez M, Cnudde V, et al (2019) Microstructural characterization of 3D printed cementitious materials. Materials (Basel) 12:. https://doi.org/10.3390/ma12182993
112. Shahmirzadi MR, Gholampour A, Kashani A, Ngo TD (2021) Shrinkage behavior of cementitious 3D printing materials: Effect of temperature and relative humidity. Cem Concr Compos 124:104238. https://doi.org/10.1016/J.CEMCONCOMP.2021.104238
113. Moelich GM, Kruger J, Combrinck R (2020) Plastic shrinkage cracking in 3D printed concrete. Compos Part B Eng 200:108313. https://doi.org/10.1016/J.COMPOSITESB.2020.108313
114. Van Der Putten J, Snoeck D, De Coensel R, et al (2021) Early age shrinkage phenomena of 3D printed cementitious materials with superabsorbent polymers. J Build Eng 35:102059. https://doi.org/10.1016/J.JOBE.2020.102059
115. Jiang C, Yang Y, Wang Y, et al (2014) Autogenous shrinkage of high performance concrete containing mineral admixtures under different curing temperatures. Constr Build Mater 61:260–269. https://doi.org/10.1016/J.CONBUILDMAT.2014.03.023
116. Gonzalez-Corominas A, Etxeberria M (2016) Effects of using recycled concrete aggregates on the shrinkage of high performance concrete. Constr Build Mater 115:32–41. https://doi.org/10.1016/J.CONBUILDMAT.2016.04.031
117. Piasta W, Zarzycki B (2017) The effect of cement paste volume and w/c ratio on shrinkage strain, water absorption and compressive strength of high performance concrete. Constr Build Mater 140:395–402. https://doi.org/10.1016/J.CONBUILDMAT.2017.02.033
118. Dueramae S, Tangchirapat W, Chindaprasirt P, et al (2020) Autogenous and drying shrinkages of mortars and pore structure of pastes made with activated binder of calcium carbide residue and fly ash. Constr Build Mater 230:116962. https://doi.org/10.1016/J.CONBUILDMAT.2019.116962
119. Federowicz K, Kaszyńska M, Zieliński A, Hoffmann M (2020) Effect of curing methods on shrinkage development in 3D-printed concrete. Materials (Basel) 13:. https://doi.org/10.3390/ma13112590
120. Shakor P, Nejadi S, Paul G (2019) A study into the effect of different nozzles shapes and fibre-reinforcement in 3D printed mortar. Materials (Basel) 12:. https://doi.org/10.3390/MA12101708
121. Slavcheva GS (2019) Drying and shrinkage of cement paste for 3D printable concrete. IOP Conf Ser Mater Sci Eng 481:. https://doi.org/10.1088/1757-899X/481/1/012043
122. Xiao J, Zou S, Ding T, et al (2021) Fiber-reinforced mortar with 100% recycled fine aggregates: A cleaner perspective on 3D printing. J Clean Prod 319:128720. https://doi.org/10.1016/J.JCLEPRO.2021.128720
123. Yu K, McGee W, Ng TY, et al (2021) 3D-printable engineered cementitious composites (3DP-ECC): Fresh and hardened properties. Cem Concr Res 143:106388. https://doi.org/10.1016/J.CEMCONRES.2021.106388
124. Panda B, Chandra Paul S, Jen Tan M (2017) Anisotropic mechanical performance of 3D printed fiber reinforced sustainable construction material. Mater Lett 209:146–149. https://doi.org/10.1016/J.MATLET.2017.07.123
125. Wolfs RJM, Bos FP, Salet TAM (2019) Hardened properties of 3D printed concrete: The influence of process parameters on interlayer adhesion. Cem Concr Res 119:132–140. https://doi.org/10.1016/J.CEMCONRES.2019.02.017

126. et al. VNN (2017) Micro-and Macroscopic Investigations on the Interface Between Layers of 3D-Printed Cementitious Elements. Proc ICACMS 2017 Int Conf Adv Constr Mater Syst 3:3–8
127. Nematollahi B, Xia M, Bong SH, Sanjayan J (2019) Hardened properties of 3D printable 'One-Part' Geopolymer for construction applications. Springer International Publishing
128. Marchment T, Xia M, Dodd E, et al (2017) Effect of delay time on the mechanical properties of extrusion-based 3D printed concrete. ISARC 2017 - Proc 34th Int Symp Autom Robot Constr 240–245. https://doi.org/10.22260/isarc2017/0032
129. Nematollahi B, Bong SH, Xia M, Sanjayan J (2020) Digital Fabrication of 'Just-Add-Water' Geopolymers: Effects of Curing Condition and Print-Time Interval. Springer International Publishing
130. Keita E, Bessaies-Bey H, Zuo W, et al (2019) Weak bond strength between successive layers in extrusion-based additive manufacturing: measurement and physical origin. Cem Concr Res 123:105787. https://doi.org/10.1016/J.CEMCONRES.2019.105787
131. Ye J, Cui C, Yu J, et al (2021) Effect of polyethylene fiber content on workability and mechanical-anisotropic properties of 3D printed ultra-high ductile concrete. Constr Build Mater 281:122586. https://doi.org/10.1016/J.CONBUILDMAT.2021.122586
132. Zhu B, Pan J, Nematollahi B, et al (2019) Development of 3D printable engineered cementitious composites with ultra-high tensile ductility for digital construction. Mater Des 181:108088. https://doi.org/10.1016/J.MATDES.2019.108088
133. Yang Y, Wu C, Liu Z, et al (2022) Mechanical anisotropy of ultra-high performance fibre-reinforced concrete for 3D printing. Cem Concr Compos 125:104310. https://doi.org/10.1016/J.CEMCONCOMP.2021.104310
134. Zhang Y, Aslani F (2021) Development of fibre reinforced engineered cementitious composite using polyvinyl alcohol fibre and activated carbon powder for 3D concrete printing. Constr Build Mater 303:124453. https://doi.org/10.1016/J.CONBUILDMAT.2021.124453
135. Baz B, Aouad G, Kleib J, et al (2021) Durability assessment and microstructural analysis of 3D printed concrete exposed to sulfuric acid environments. Constr Build Mater 290:123220. https://doi.org/10.1016/J.CONBUILDMAT.2021.123220
136. Zhang Y, Zhang Y, Yang L, et al (2021) Hardened properties and durability of large-scale 3D printed cement-based materials. Mater Struct Constr 54:. https://doi.org/10.1617/s11527-021-01632-x
137. Blaakmeer J, Lobo B (2020) A Robust Mortar and Printing System. Springer International Publishing
138. Van Der Putten J, Azima M, Van den Heede P, et al (2020) Neutron radiography to study the water ingress via the interlayer of 3D printed cementitious materials for continuous layering. Constr Build Mater 258:119587. https://doi.org/10.1016/J.CONBUILDMAT.2020.119587
139. Van Der Putten J, De Volder M, Van den Heede P, et al (2022) Transport properties of 3D printed cementitious materials with prolonged time gap between successive layers. Cem Concr Res 155:106777. https://doi.org/10.1016/J.CEMCONRES.2022.106777
140. Sanjayan JG, Nematollahi B, Xia M, Marchment T (2018) Effect of surface moisture on inter-layer strength of 3D printed concrete. Constr Build Mater 172:468–475. https://doi.org/10.1016/J.CONBUILDMAT.2018.03.232
141. Bran Anleu PC, Wangler T, Flatt RJ (2018) Chloride ingress through cold joints in digitally fabricated concrete by micro-XRF mapping. In: 1st RILEM International Conference on Concrete and Digital Fabrication (DigitalConcrete 2018)
142. Sikora P, Techman M, Federowicz K, et al (2022) Insight into the microstructural and durability characteristics of 3D printed concrete: Cast versus printed specimens. Case Stud Constr Mater 17:e01320. https://doi.org/10.1016/J.CSCM.2022.E01320
143. Assaad JJ, Hamzeh F, Hamad B (2020) Qualitative assessment of interfacial bonding in 3D printing concrete exposed to frost attack. Case Stud Constr Mater 13:e00357. https://doi.org/10.1016/J.CSCM.2020.E00357
144. Sanchez AMA, Wangler T, Stefanoni M, Angst U (2022) Microstructural examination of carbonated 3D-printed concrete. J Microsc 286:141–147. https://doi.org/10.1111/jmi.13087
145. Sun J, Aslani F, Lu J, et al (2021) Fibre-reinforced lightweight engineered cementitious composites for 3D concrete printing. Ceram Int 47:27107–27121. https://doi.org/10.1016/J.CERAMINT.2021.06.124
146. Voigt T, Mbele J-J, Wang K, Shah SP (2010) Using Fly Ash, Clay, and Fibers for Simultaneous Improvement of Concrete Green Strength and Consolidatability for Slip-Form Pavement. J Mater Civ Eng 22:196–206. https://doi.org/10.1061/(asce)0899-1561(2010)22:2(196)
147. Chen Y, Romero Rodriguez C, Li Z, et al (2020) Effect of different grade levels of calcined clays on fresh

and hardened properties of ternary-blended cementitious materials for 3D printing. Cem Concr Compos 114:103708. https://doi.org/10.1016/j.cemconcomp.2020.103708
148. Panda B, Ruan S, Unluer C, Tan MJ (2019) Improving the 3D printability of high volume fly ash mixtures via the use of nano attapulgite clay. Compos Part B Eng 165:75–83. https://doi.org/10.1016/J.COMPOSITESB.2018.11.109
149. Panda B, Unluer C, Tan MJ (2018) Investigation of the rheology and strength of geopolymer mixtures for extrusion-based 3D printing. Cem Concr Compos 94:307–314. https://doi.org/10.1016/J.CEMCONCOMP.2018.10.002
150. Zhang Y, Zhang Y, Liu G, et al (2018) Fresh properties of a novel 3D printing concrete ink. Constr Build Mater 174:263–271. https://doi.org/10.1016/J.CONBUILDMAT.2018.04.115
151. Bai G, Wang L, Ma G, et al (2021) 3D printing eco-friendly concrete containing under-utilised and waste solids as aggregates. Cem Concr Compos 120:104037. https://doi.org/10.1016/J.CEMCONCOMP.2021.104037
152. Sambucci M, Valente M, Sibai A, et al (2020) Rubber-Cement Composites for Additive Manufacturing: Physical, Mechanical and Thermo-Acoustic Characterization. Springer International Publishing
153. Cuevas K, Chougan M, Martin F, et al (2021) 3D printable lightweight cementitious composites with incorporated waste glass aggregates and expanded microspheres – Rheological, thermal and mechanical properties. J Build Eng 44:102718. https://doi.org/10.1016/J.JOBE.2021.102718
154. Ding T, Xiao J, Zou S, Yu J (2021) Flexural properties of 3D printed fibre-reinforced concrete with recycled sand. Constr Build Mater 288:123077. https://doi.org/10.1016/J.CONBUILDMAT.2021.123077
155. Dorn T, Hirsch T, Stephan D (2020) Study on the Influence of Accelerators on the Hydration of Portland Cement and Their Applicability in 3D Printing. Springer International Publishing
156. Khalil N, Aouad G, El Cheikh K, Rémond S (2017) Use of calcium sulfoaluminate cements for setting control of 3D-printing mortars. Constr Build Mater 157:382–391. https://doi.org/10.1016/J.CONBUILDMAT.2017.09.109
157. Chen M, Guo X, Zheng Y, et al (2018) Effect of tartaric acid on the printable, rheological and mechanical properties of 3D printing sulphoaluminate cement paste. Materials (Basel) 11:. https://doi.org/10.3390/ma11122417
158. Deshmukh AS, Heintzkill RT, Huerta RA, Sobolev K (2021) Rheological response of magnetorheological cementitious inks tuned for active control in digital construction. ACI Mater J 118:263–274. https://doi.org/10.14359/51733128
159. Shilton R, Wang S, Banthia N (2025) Use of polysaccharides as a rheology modifying admixture for alkali activated materials for 3D printing. Constr Build Mater 458:139661. https://doi.org/10.1016/j.conbuildmat.2024.139661
160. Zhang N, Sanjayan J (2023) Mechanisms of rheological modifiers for quick mixing method in 3D concrete printing. Cem Concr Compos 142:105218. https://doi.org/10.1016/j.cemconcomp.2023.105218
161. Falliano D, De Domenico D, Ricciardi G, Gugliandolo E (2020) 3D-printable lightweight foamed concrete and comparison with classical foamed concrete in terms of fresh state properties and mechanical strength. Constr Build Mater 254:119271. https://doi.org/10.1016/J.CONBUILDMAT.2020.119271
162. Li Z, Wang L, Ma G (2020) Mechanical improvement of continuous steel microcable reinforced geopolymer composites for 3D printing subjected to different loading conditions. Compos Part B Eng 187:107796. https://doi.org/10.1016/J.COMPOSITESB.2020.107796
163. Perrot A, Jacquet Y, Rangeard D, et al (2020) Nailing of layers: A promisingway to reinforce concrete 3D printing structures. Materials (Basel) 13:. https://doi.org/10.3390/ma13071518
164. Geneidy O, Kumarji S, Dubor A, Sollazzo A (2020) Simultaneous reinforcement of concrete while 3D printing. In: Second RILEM International Conference on Concrete and Digital Fabrication: Digital Concrete 2020 2. Springer, pp 895–905
165. Marchment T, Sanjayan J (2020) Mesh reinforcing method for 3D Concrete Printing. Autom Constr 109:102992. https://doi.org/10.1016/J.AUTCON.2019.102992
166. Itim A, Ezziane K, Kadri EH (2011) Compressive strength and shrinkage of mortar containing various amounts of mineral additions. Constr Build Mater 25:3603–3609. https://doi.org/10.1016/J.CONBUILDMAT.2011.03.055
167. Ting GHA, Tay YWD, Qian Y, Tan MJ (2019) Utilization of recycled glass for 3D concrete printing: rheological and mechanical properties. J Mater Cycles Waste Manag 21:994–1003. https://doi.org/10.1007/s10163-019-00857-x
168. Hambach M, Rutzen M, Volkmer D (2019) Properties of 3D-Printed Fiber-Reinforced Portland Cement

Paste. 3D Concr Print Technol 73–113. https://doi.org/10.1016/B978-0-12-815481-6.00005-1

169. Bos F, Dezaire S, Ahmed Z, et al (2020) Bond of reinforcement cable in 3D printed concrete. In: Second RILEM International Conference on Concrete and Digital Fabrication: Digital Concrete 2020 2. Springer, pp 584–600
170. Katzer J, Szatkiewicz T (2019) Properties of concrete elements with 3-D printed formworks which substitute steel reinforcement. Constr Build Mater 210:157–161. https://doi.org/10.1016/J.CONBUILDMAT.2019.03.204
171. García de Soto B, Agustí-Juan I, Hunhevicz J, et al (2018) Productivity of digital fabrication in construction: Cost and time analysis of a robotically built wall. Autom Constr 92:297–311. https://doi.org/10.1016/J.AUTCON.2018.04.004
172. Nerella VN, Krause M, Mechtcherine V (2020) Direct printing test for buildability of 3D-printable concrete considering economic viability. Autom Constr 109:102986. https://doi.org/10.1016/J.AUTCON.2019.102986
173. Batikha M, Jotangia R, Baaj MY, Mousleh I (2022) 3D concrete printing for sustainable and economical construction: A comparative study. Autom Constr 134:104087. https://doi.org/10.1016/J.AUTCON.2021.104087
174. Yao Y, Hu M, Di Maio F, Cucurachi S (2020) Life cycle assessment of 3D printing geo-polymer concrete: An ex-ante study. J Ind Ecol 24:116–127
175. Alhumayani H, Gomaa M, Soebarto V, Jabi W (2020) Environmental assessment of large-scale 3D printing in construction: A comparative study between cob and concrete. J Clean Prod 270:122463
176. Mohammad M, Masad E, Al-Ghamdi SG (2020) 3D Concrete Printing Sustainability : A Comparative. Buildings 10:
177. Weng Y, Li M, Ruan S, et al (2020) Comparative economic, environmental and productivity assessment of a concrete bathroom unit fabricated through 3D printing and a precast approach. J Clean Prod 261:121245
178. Markin V, Krause M, Otto J, et al (2021) 3D-printing with foam concrete: From material design and testing to application and sustainability. J Build Eng 43:102870
179. Tobi ALM, Omar SA, Yehia Z, et al (2018) Cost viability of 3D printed house in UK. In: IOP Conference Series: Materials Science and Engineering. IOP Publishing, p 12061
180. Long W-J, Tao J-L, Lin C, et al (2019) Rheology and buildability of sustainable cement-based composites containing micro-crystalline cellulose for 3D-printing. J Clean Prod 239:118054
181. Kantumuchu VC (2021) Additive Manufacturing for Industrial Applications and Potential Quality Challenges. Adv Addit Manuf Process Bentham Sci Publ Bussum, Netherlands 216–239

Statements & Declarations

Funding: ***The authors declare that no funds, grants, or other support were received during the preparation of this manuscript.***

Competent Interest: ***The authors have no relevant financial or non-financial interests to disclose.***